

## Article

# Description of *Aliinostoc alkaliphilum* sp. nov. (Nostocales, Cyanobacteria), a New Bioactive Metabolite-Producing Strain from Salina Verde (Pantanal, Brazil) and Taxonomic Distribution of Bioactive Metabolites in *Nostoc* and *Nostoc*-like Genera

Maria Christodoulou <sup>1,\*</sup> , Jouni Jokela <sup>1</sup> , Matti Wahlsten <sup>1</sup> , Lyudmila Saari <sup>1</sup>, Athena Economou-Amilli <sup>2</sup>, Marli de Fatima Fiore <sup>3</sup>  and Kaarina Sivonen <sup>1</sup>

<sup>1</sup> Department of Microbiology, Faculty of Agriculture and Forestry, University of Helsinki, P.O. Box 56, 00014 Helsinki, Finland

<sup>2</sup> Department of Ecology and Systematics, Faculty of Biology, National and Kapodistrian University of Athens, 15784 Athens, Greece

<sup>3</sup> Laboratory of Cellular and Molecular Biology, Center for Nuclear Energy in Agriculture, University of São Paulo, Piracicaba 13416-000, São Paulo, Brazil

\* Correspondence: maria.christodoulou@helsinki.fi



**Citation:** Christodoulou, M.; Jokela, J.; Wahlsten, M.; Saari, L.; Economou-Amilli, A.; Fiore, M.d.F.; Sivonen, K. Description of *Aliinostoc alkaliphilum* sp. nov. (Nostocales, Cyanobacteria), a New Bioactive Metabolite-Producing Strain from Salina Verde (Pantanal, Brazil) and Taxonomic Distribution of Bioactive Metabolites in *Nostoc* and *Nostoc*-like Genera. *Water* **2022**, *14*, 2470. <https://doi.org/10.3390/w14162470>

Academic Editor: Armah A. de la Cruz

Received: 22 June 2022

Accepted: 5 August 2022

Published: 10 August 2022

**Publisher's Note:** MDPI stays neutral with regard to jurisdictional claims in published maps and institutional affiliations.



**Copyright:** © 2022 by the authors. Licensee MDPI, Basel, Switzerland. This article is an open access article distributed under the terms and conditions of the Creative Commons Attribution (CC BY) license (<https://creativecommons.org/licenses/by/4.0/>).

**Abstract:** Cyanobacteria are a group of oxygenic photosynthetic prokaryotes found in almost all habitats on earth including those characterized as extreme environments. It has been observed that the number of studies dealing with the biodiversity of extremophilic cyanobacteria is limited while studies exploring their bioactive potential are even scarcer. The taxonomy of three *Nostoc*-like cyanobacterial strains isolated from a shallow lake in Brazil was studied by applying a polyphasic approach. The bioactive potential of the strains was also evaluated using antimicrobial susceptibility testing. The metabolites present in the bioactive HPLC fractions were identified by UPLC/ESI/Q-TOF. Based on our phylogenetic inferences in combination with morphological and ecological information, we describe *Aliinostoc alkaliphilum* sp. nov., exhibiting antibacterial and antifungal activities. The main bioactive metabolite in all three strains was nocuolin A, which represents the first report of this metabolite in *Aliinostoc*. Our phylogenetic studies also revealed that many bioactive metabolite-producing strains that are currently assigned to *Nostoc* belong to other distinct evolutionary lineages. These findings highlight the importance of polyphasic approach studies in both cyanobacterial taxonomy and natural product discovery programs.

**Keywords:** *Aliinostoc*; cyanobacteria; polyphasic approach; bioactive compounds; nocuolin A; Salina Verde

## 1. Introduction

Cyanobacteria represent a group of morphologically diverse oxyphototrophic bacteria found in almost all habitats on Earth including those which are considered hostile to life and are known as 'extreme' environments [1].

The immense diversity of cyanobacteria refers not only to their morphological variability and habitat preferences but also to a variety of functionally diverse and structurally complex metabolites they produce [2,3]. A result of this high degree of chemical diversity is the increased possibility of discovering substances with biomedically interesting properties in cyanobacteria [4]. Indeed, over 2000 metabolites have been identified from cyanobacteria thus far, most of which derive from genera such as *Nostoc* and *Lyngbya* [5]. This highly uneven taxonomic distribution of cyanobacterial metabolites has already been highlighted in previous studies including Leão et al. [6] and Engene et al. [7–12]. According to the same studies, the major reason for this phenomenon is the classification of cyanobacteria based

solely on morphological diagnostic features, thus resulting in a significant underestimation of cyanobacterial diversity [6–12]. This morphology-only based approach, which was traditionally used in cyanobacterial taxonomy, is nowadays replaced by a modern system in which new taxa are described based on a combination of morphological, ultrastructural, molecular and ecological data. This ‘polyphasic approach’ led not only to the establishment of several new monophyletic taxa [13–15] but also allowed for more targeted natural product discovery efforts [8–10].

*Nostoc*, with *Nostoc commune* as its type species, is one of the most well-known, cosmopolitan cyanobacterial genera [16]. Despite being one of the earliest cyanobacterial genera described, its taxonomy remains problematic due to the lack of clear morphological traits [17]. Recent phylogenetic studies have shown that *Nostoc* is polyphyletic and several new *Nostoc*-like genera including *Mojavia* [16], *Desmonostoc* [18], *Halotia* [19], *Komarekiella* [20], *Aliinostoc* [21], *Desikacharya* [17], *Compactonostoc* [22], *Parakomarekiella* [23] and *Pseudoaliinostoc* [24] have already been established. Nevertheless, existing phylogenetic studies reveal that many other strains assigned to *Nostoc* fall outside the *Nostoc sensu stricto* clade hosting the generitype, indicating the need for further taxonomic revision of this genus [20].

In addition to its genetic heterogeneity, strains assigned to *Nostoc* have been reported to produce a variety of natural products ranging from toxins [25,26] to biologically active molecules [2,27,28], suggesting that *Nostoc* is a prolific source of bioactive compounds [29–31]. Approximately 12.0% of the cyanobacterial natural products included in CyanoMetDB [5] are ascribed to more than 60 different ‘*Nostoc*’ strains. Interestingly, most of these bioactive compound-producing strains were identified solely based on phenotypic characteristics or have been initially classified as ‘*Nostoc*’ based on partial 16S rRNA gene sequencing data pending further studies to confirm their taxonomic placement.

*Nostoc*-like strains have been isolated from a wide range of habitats including alkaline lakes, which represent a unique and stable environment characterized by high pH levels that host unique microbial communities [32]. Alkaline lakes with varying salinity levels are found worldwide, predominantly in arid and semi-arid regions [33,34] including the Brazilian Pantanal, the world’s largest tropical wetland, which has hundreds of shallow lakes that vary greatly in abiotic parameters such as pH and salinity and coexist in proximity [35]. Salina Verde is a shallow saline-alkaline lake (water level ranging between 0.1 m to 1.5 m) located in the Aquidauana municipality of the Brazilian state of Mato Grosso do Sul and occupies an area of 0.15 km<sup>2</sup> [36]. The almost permanent cyanobacterial bloom observed in this lake is dominated by *Anabaenopsis elenkinii* [34]. Heterocytous cyanobacteria isolated from Brazilian alkaline lakes including Salina Verde were studied by Genuário et al. [37] using a polyphasic approach. The morphological and phylogenetic analysis conducted therein revealed, inter alia, the existence of a novel cyanobacterial lineage (Cluster II in their analysis) that was morphologically similar but phylogenetically distant from *Nostoc sensu stricto* clade [37]. The cluster was characterized by the presence of motile hormogonia with gas vesicles that was considered an autapomorphic diacritical feature separating this cluster from other heterocytous genera [37]. With this information in hand and the application of a polyphasic approach, Bagchi et al. [21] described the new *Nostoc*-like genus *Aliinostoc* (type strain; *A. morphoplasticum* NOS) from an eutrophic pond in India and suggested the classification of the above mentioned strains under this novel genus. Since then, two more *Aliinostoc* species (*A. magnakinetifex* and *A. catenatum*) isolated from soil habitats in Iran were established using a polyphasic approach [38]. These three taxa are the only validly described *Aliinostoc* species and none of them have been studied in respect to their bioactive potential.

The aim of this study is to expand the ecological and geographical distribution of *Aliinostoc* with the establishment of *Aliinostoc alkaliphilum* sp. nov. from Salina Verde (Pantanal wetland, Brazil) based on a polyphasic approach. Furthermore, this study explores the bioactive potential of the new species against bacterial and fungal potential pathogens as part of our ongoing efforts to discover novel bioactive metabolites with pharmaceutical

applications. Finally, this study utilizes all available genetic (16S rRNA gene; NCBI) and bioactive metabolite information (CyanoMetDB; [5]) to investigate whether genus *Nostoc* is indeed rich in bioactive compounds or whether this perceived chemical richness of *Nostoc* emerges from the lack of proper taxonomic studies based on the abovementioned polyphasic approach.

## 2. Materials and Methods

### 2.1. Microbial Strains, Microbiological Media and Growth Conditions

#### 2.1.1. Cyanobacteria

Cyanobacterial strains CENA513, CENA514 and CENA524, initially classified as *Nostoc* sp. [37], were used in this study. These three strains were isolated from water samples collected from Salina Verde saline-alkaline lake (municipality of Aquidauana, Nhecolandia region, state of Mato Grosso do Sul) as previously described [37]. The lake is generally characterized by relatively high pH levels (8.4–9.7) and electrical conductivity values ranging between 1.98 and 15 mS cm<sup>-1</sup> during the wet and dry seasons, respectively [36]. All strains were grown on solid and in liquid Z8 medium without nitrogen source [39]. Liquid cultures were maintained in an incubator shaker (Climo-Shaker ISF1-X, Kuhner) at 18 °C under constant illumination with white fluorescent light (18.65 μmol of photons s<sup>-1</sup> m<sup>-2</sup>) and 100 rpm shaking speed or without shaking. Strain CENA513 was purified using previously described methods [40] and was used to confirm the cyanobacterial origin of the produced bioactive metabolites. For the bioactivity assays, strains were grown in 5L Erlenmeyer flasks containing 2.5 L of Z8 liquid media without nitrogen source under constant illumination of 10–15 μmol of photons s<sup>-1</sup> m<sup>-2</sup> and permanent sterile aeration at 18 °C for 30 days. Cells were harvested by centrifugation at 9000 × g for 10 min at room temperature (RT) and were stored at –20 °C until lyophilization.

#### 2.1.2. Bacteria and Fungi

All bacterial and fungal strains used in the present study were obtained from HAMBI (University of Helsinki, Department of Microbiology) microbial culture collection (<https://www.helsinki.fi/en/infrastructures/biodiversity-collections/infrastructures/microbial-domain-biological-resource-centre-hambi> (accessed on 17 May 2019)). These included the non-antibiotic resistant strains *Staphylococcus aureus* HAMBI 66, *Enterococcus faecium* HAMBI 1821, *Bacillus cereus* HAMBI 1881, *Micrococcus luteus* HAMBI 2688, *Pseudomonas aeruginosa* HAMBI 25, *Acinetobacter baumannii* HAMBI 1760, *Enterobacter aerogenes* HAMBI 1898, *Salmonella enterica* HAMBI 2331, *Candida albicans* HAMBI 484, *C. krusei* HAMBI 486, *C. parapsilosis* HAMBI 487, *Cryptococcus neoformans* HAMBI 488, *Mucor* sp. HAMBI 831 and *Aspergillus flavus* HAMBI 829. Three different solid media, i.e., Mueller–Hinton (MH), Mueller Hinton supplemented with 2% glucose and 0.5 μg mL<sup>-1</sup> methylene blue (MH-GMB) and potato-dextrose (PDA) solid media, were used during antimicrobial susceptibility assays, and were prepared according CLSI guidelines as previously described [41]. All bacterial and yeast strains were grown overnight at 28 or 37 °C, whereas filamentous fungi were grown on solid media for three days at 28 °C (see Supplementary Table S1 for details).

#### 2.2. Microscopy

Three cyanobacterial strains, growing in liquid Z8 media without nitrogen source, were studied under a Leica MZ6 Stereomicroscope (Wetzlar, Germany) and a Zeiss Axioskop 2 plus Light Microscope (Jena, Germany). Light photomicrographs were acquired using an AxioCam 305 color digital camera and processed using ZEISS ZEN 2.6 (blue edition) software. Presence of sheath was confirmed by staining with India ink. We analyzed the shape and size of trichomes and vegetative cells in at least 20 trichomes from each strain, summarizing 50 cells. The shape, size and position of heterocytes and akinetes as well as the presence of hormogonia were also recorded and compared to data available for *Aliinostoc* species. *Aliinostoc* strains for which morphological assessment is missing were not included in the comparison.

Strain CENA513 was further studied by means of scanning electron microscopy (SEM) and transmission electron microscopy (TEM). For SEM observations, lyophilized cells were affixed to aluminum stubs using double-sided carbon tape, were spray coated in gold-palladium and observed under a JEOL JSM 35 Scanning Electron Microscope (Tokyo, Japan) operating at 19 kV. For TEM studies, cells were first immobilized in sodium alginate beads as described by Romo and Perez-Martinez [42] and were allowed to grow for 25 days in Z8 liquid media without nitrogen source as described above. Following this step, cells entrapped in alginate beads were fixed with 2.5% (*v/v*) glutaraldehyde solution in 0.1 M sodium cacodylate buffer for 3 h at RT and post-fixed in 1% (*w/v*) osmium tetroxide in the same buffer for 1 h. The specimen was dehydrated in a graded ethanol series (50, 70, 96 and 100%) and washed twice in propylenoxide. Sample was then embedded in two mixtures of low viscosity resin and propylenoxide (30% and 70%) and finally in low viscosity resin. Surface sections were stained with 2% uranyl acetate and lead citrate as described by Reynolds [43] and examined using a Jeol JEM-1400 Transmission Electron Microscope operating at 80 kV at the Electron Microscopy Unit of the Institute of Biotechnology (EMBI, University of Helsinki, Finland).

### 2.3. Molecular Characterization

#### 2.3.1. DNA Extraction, PCR Amplification and Sequencing

The 16S rRNA nucleotide sequences were previously obtained [37] and were publicly available through NCBI (KX458483, KX458484, KX458485).

For the study of 16S-23S Internal Transcribed Spacer (ITS) region, total genomic DNA from all strains was extracted using the E.Z.N.A. Plant DNA Kit (Omega Bio-tek, Inc., Norcross, GA, USA) according to the manufacturer's protocol with some modifications that are presented below. During the first step of extraction, cyanobacterial biomass was transferred to a 2 mL screw cap tube together with SP1 buffer and sterile acid-washed glass beads (425–600  $\mu\text{m}$ ; Sigma-Aldrich). Cells were then disrupted using a FastPrep-24<sup>®</sup> cell disrupter (MP Biomedicals, Santa Ana, CA, USA) two times for 20 s at a speed of 6.5  $\text{m s}^{-1}$  at RT. Following this step, RNase was added to the extracts, samples were mixed and incubated at 65 °C for 1 h. Partial 16S and the 16S-23S ITS region were amplified using the cyanobacteria-specific primers P5 5'-TGTACACACCGCCCGTC-3' sensu Boyer et al. [44] and 23S30R 5'-CTTCGCCTCTGTGTGCCTAGGT-3' after Taton et al. [45]. The PCR reactions were prepared in 50  $\mu\text{L}$  aliquots containing 1X Q5 reaction buffer (New England Biolabs), 0.2 mM of each deoxynucleotide triphosphates (dNTPs; Thermo Scientific, Waltham, MA, USA), 0.5  $\mu\text{M}$  of each of the primers (Sigma-Aldrich), 0.02 U of Q5 High-Fidelity DNA Polymerase (New England Biolabs) and 90–100 ng of genomic DNA, determined using NanoDrop One/One Microvolume UV-Vis Spectrophotometer (Thermo Scientific). Amplifications were run in a BioRad iCycler thermal cycler. The profile used included an initial denaturation step at 98 °C for 30 s, followed by 35 cycles of denaturation at 98 °C for 10 s, annealing at 65 °C for 30 s and extension at 72 °C for 2 min and a final extension step of 2 min at 72 °C.

PCR products were analyzed on a 2.0% (*w/v*) agarose gel stained with EtBr. Two PCR fragments differing by approximately 300 bp were present in all reactions. Both fragments were gel-purified using the Nucleospin Gel and PCR clean up kit (Macherey-Nagel) and sequenced using BigDye Terminator v3.1 Cycle Sequencing Kit on an ABI 3730xl DNA analyser (Applied Biosystems) using the same primer pair as in PCR amplification. Sequencing was carried out at the Sequencing Unit of Institute for Molecular Medicine Finland (FIMM) Technology Center. The generated sequences were edited with CodonCode Aligner v.9.0.1 (CodonCode Corporation, Barnstable, MA, USA) and consensus sequences were obtained. The sequences were deposited in GenBank database under the accession numbers OK042916-OK042921.

### 2.3.2. Phylogenetic Analysis of 16S rRNA

Sequences were evaluated for their homology to publicly available 16S rRNA genes of cyanobacteria through a BLASTn search in the National Center for Biotechnology Information (NCBI) database. The compiled dataset included taxa sharing  $\geq 97\%$  16S rRNA sequence identity with the studied strains, bioactive metabolite-producing *Nostoc* strains and representatives of morphologically similar genera (231 taxa including the outgroup). All selected sequences were at least 1100 bp long. *Synechococcus elongatus* PCC 6301 (NR\_074309) was used as the outgroup. Multiple sequence alignment was performed using ClustalX version 2.1 [46]. The Akaike Information Criterion [47] as implemented in jModeltest v.2.1.10 [48] was used to choose the best-fit model of DNA substitution. The model GTR + I + G was selected for Bayesian Inference (BI), which was carried out in MrBayes v.3.2.6 [49]. For this analysis, two runs with four chains each (one cold and three heated chains) were run simultaneously for  $25 \times 10^6$  Markov Chain Monte Carlo (MCMC) generations starting with a random tree. Sampling frequency was every 1000th generation. The average standard deviation between the two MCMC runs was below 0.01, indicating convergence. The first 25% of trees was discarded as burn-in and a 50% majority rule consensus tree was calculated including posterior probabilities. ML analysis was performed using the web IQ-Tree (<http://iqtree.cibiv.univie.ac.at/> (accessed on 15 April 2022) [50]), using automatic model selection (selected model; TVMe + I + G4) and 1000 bootstrap replicates. The phylogenetic trees were visualized using FigTree v1.4.2 (created by Andrew Rambaut, Edinburgh, UK, <http://tree.bio.ed.ac.uk/software/figtree> (accessed on 20 April 2022)) and re-drawn in Inkscape v0.48.4 (created by Inkscape Developer Team, Boston, MA, USA, [www.inkscape.org](http://www.inkscape.org) (accessed on 20 April 2022)). All taxa used in the phylogenetic analyses and their GenBank accession numbers are presented in Table S2. A distance matrix was also calculated in MEGA 11 [51] using the Kimura-2 parameter model [52].

### 2.3.3. Determination of 16S-23S rRNA ITS Secondary Structures

Identification of conserved 16S-23S rRNA intergenic spacer (ITS) regions was carried out according to Itean et al. [53]. Hypothetical secondary structures of D1-D1' and Box B were predicted using Mfold web server [54] by applying the default conditions except from the draw mode that was set to 'Untangle with loop fix', choosing secondary structures with minimum free energy ( $\Delta G$ ). The obtained structures were compared with the available homologous structures of the known *Aliinostoc* species. Although we obtained operons with both tRNAs and with no tRNAs in all *Aliinostoc alkaliphilum* strains, comparison included operons with no tRNAs only. All figures were edited in Adobe Photoshop v.23.2.0 (Adobe Systems Inc., San Jose, CA, USA).

## 2.4. Bioassays

### 2.4.1. Preparation of Extracts

For antimicrobial susceptibility tests, 500 mg of freeze-dried biomass from each strain was transferred in five 2 mL screw-cap tubes (100 mg per tube) together with glass beads (0.5 mm diameter, Scientific Industries Inc., Bohemia, New York, NY, USA) and 1 mL of 100% LC/MS grade methanol (MeOH; Merck, Darmstadt, Germany). Cells were disrupted using a FastPrep-24<sup>®</sup> cell disrupter (MP Biomedicals, Santa Ana, CA, USA) two times for 20 s at a speed of  $6.5 \text{ m s}^{-1}$  at RT. Intracellular bioactive compounds were obtained after centrifugation at  $10,000 \times g$  for 5 min at RT. Supernatants from each strain were pooled and solvent was evaporated under  $\text{N}_2$  flow. Extracts were re-solubilized in 5 mL of 100% MeOH and stored at  $-20^\circ \text{C}$  until further evaluation.

### 2.4.2. Antimicrobial Disk Diffusion Susceptibility Testing

Sterile blank paper disks (Abtek Biologicals Ltd.; Liverpool, UK) were aseptically transferred in 96-well polystyrene microplates (F-bottom; Greiner Bio One, Kremsmünster, Austria). Following this step, 300  $\mu\text{L}$  of crude extract (corresponding to 30 mg of freeze-dried biomass) was transferred on each disk and allowed to air-dry overnight. Disks

containing 300  $\mu\text{L}$  of 100% MeOH were used as negative controls in both bacterial and fungal bioassays. Kanamycin 1000 mg antibiotic disks (REF 03-KAN1000, Abtek Biologicals Ltd.; Liverpool, UK) were used as a positive control in bacterial bioassays, whereas disks containing 50  $\mu\text{L}$  of nystatin solution (Sigma-Aldrich, St. Louis, MO, USA, stock solution; 1  $\text{mg mL}^{-1}$  dissolved in 70% MeOH (*v/v*)) were used as positive controls in all fungal bioassays. All disk diffusion assays were performed following the CLSI guidelines as described in the CLSI document M02-A11 [55] and Leber [41]. Plates were incubated overnight (bacteria and yeast) or for 72 h (filamentous fungi) and inhibition zones (including paper disk diameter) were recorded.

## 2.5. Liquid Chromatography

### 2.5.1. Fractionation of Extracts by High-Performance Liquid Chromatography (HPLC)

Two grams of freeze-dried cell biomass were extracted twice with 60 mL of 100% MeOH using a Heidolph Silent Crusher M (Schwabach, Germany) at 20,000 rpm for 30 s. Samples were centrifuged at  $10,000\times g$  for 5 min at RT and supernatants from each strain were combined in a round bottom flask. Cell components and highly hydrophobic compounds were removed by solid phase extraction (SPE); the cartridges used were the commercially available C18 SPE cartridges (Phenomenex, 5 g, 20 mL Giga tubes). Following this step, samples were collected in round bottom flasks and cartridges were washed with 30 mL of MeOH 80% (*v/v*). Methanol was removed by evaporation using a Büchi rotary evaporator (Flawil, Switzerland) followed by lyophilization to remove water.

The lyophilized samples were subjected to reverse phase HPLC using an Agilent HP 1100 Series High-Performance Liquid Chromatography system (Agilent technologies, Palo Alto, CA, USA) equipped with diode array detector (DAD). Two solvents were used in the analysis: solvent A was 0.1% ammonium formate (Sigma-Aldrich, St. Louis, MO, USA) in MQ water and solvent B was HPLC grade acetonitrile (ACN) 100% (VWR Chemicals, Darmstadt, Germany). Prior to analysis, all lyophilized samples were dissolved in 4 mL of HPLC eluent mixture consisting of 50% of solvent A and 50% of solvent B. All samples were mixed well and then sonicated for 10 s in a Bandelin Sonorex super 10P ultrasonic bath (Berlin, Germany) at RT. Following this step, samples were centrifuged at full speed ( $16,100\times g$ ) for 5 min, supernatant from each sample was transferred to a 4 mL amber glass vial and stored at  $-20\text{ }^{\circ}\text{C}$  until further analysis. Metabolites were separated on a Luna<sup>®</sup> C18(2) column ( $150\times 4.60\text{ mm}$ ,  $5\text{ }\mu\text{m}$ ,  $100\text{ \AA}$ , Phenomenex, Torrance, CA, USA). Separation was achieved using the two solvents (A and B) in a linear gradient at a temperature of  $30\text{ }^{\circ}\text{C}$ . In detail, concentration of solvent B was increased from 50% to 100% in 20 min, flow rate was 1.0 mL per minute and the elution strength of B was held at 100% for another 10 min to ensure that all compounds were eluted from the column. The entire amount of each sample was injected into the column in 50  $\mu\text{L}$  batches, and each fraction was collected in separate glass test tubes. Fractions eluting at the same time were combined before solvent evaporation. Both the organic solvents and water were removed as described above. The lyophilized fractions were dissolved in 4 mL of methanol 100%, transferred to clean 4 mL amber glass vials and stored at  $-20\text{ }^{\circ}\text{C}$  until further analysis. HPLC fractions were used in disk diffusion assays as described above. Crude extract, kanamycin (bacteria) and nystatin (fungi) were used as positive controls, whereas methanol 100% was used as a negative control.

### 2.5.2. Chemical Analysis and Identification of Bioactive Metabolites

Crude extracts and bioactive fractions were analyzed using an Acquity UPLC system (Waters, Manchester, UK), equipped with a Kinetex<sup>®</sup> C8 LC column ( $50\times 2.1\text{ mm}$ ,  $1.7\text{ }\mu\text{m}$ ,  $100\text{ \AA}$ , Phenomenex, Torrance, CA, USA). UPLC was operated with a flow rate of  $0.3\text{ mL min}^{-1}$  in a gradient mode, at a temperature of  $40\text{ }^{\circ}\text{C}$ . The two solvents used in the analysis were 0.1% formic acid (Fluka, Sigma-Aldrich, St. Louis, MO, USA) in MQ water as solvent A and 0.1% formic acid in acetonitrile-isopropanol (1:1) as solvent B. In all cases, the strength of solvent B was increased from 5% to 100% in 5 min. Injection volume

was 1.0  $\mu\text{L}$ . Mass spectra were recorded with a Waters Synapt G2-Si mass spectrometer (Waters, Manchester, UK) and measurements were performed using negative and positive electrospray ionization (ESI) in resolution mode. Ions were scanned in a range from  $m/z$  50 to 2000 and UV detector range from 210 to 800 nm. Mass spectrometry (MS) analyses were performed with scan times of 0.1 s. Capillary voltage was 2.5 kV, source temperature was 120  $^{\circ}\text{C}$ , sampling cone was 40.0, source offset was 80.0, desolvation temperature was 600  $^{\circ}\text{C}$ , desolvation gas flow was 1000  $\text{L h}^{-1}$  and nebulizer gas flow was 6.5 bar. Leucine-enkephalin was used as a lock mass reference compound and calibration was carried out with sodium formate and Ultramark 1621<sup>®</sup>. UV data were also collected from 210 to 800 nm. The elemental compositions of bioactive metabolites were used for conducting an extensive search in online databases such as SciFinder<sup>®</sup> and identify the bioactive molecules. Chemical structures from all identified compounds were drawn using ChemDraw Professional v.17.0 software (PerkinElmer informatics Inc., Waltham, MA, USA).

### 2.5.3. Identification of Bioactive Metabolite-Producing ‘*Nostoc*’ Strains

CyanoMetDB [5] was used as a reference point in order to identify bioactive metabolite-producing ‘*Nostoc*’ strains. Data were visualized using R and edited using Adobe Photoshop v.23.2.0 (Adobe Systems Inc., San Jose, CA, USA) The 16S rRNA gene nucleotide sequences associated with the bioactive metabolite-producing strains were obtained from NCBI.

## 3. Results

### 3.1. Taxonomic Analysis

Description of *Aliinostoc alkaliphilum* sp. nov. under the Provisions of the International Code of Nomenclature for Algae, Fungi and Plants

*Aliinostoc alkaliphilum* Christodoulou, Economou-Amilli, Fiore et Sivonen sp. nov.

**Description** (Figures 1 and 2).

On solid media, colonies are irregular, dark brown in color with no distinct periderm. In liquid media, filaments form small clusters that are loosely attached to the bottom of the flasks. Filaments are long and flexuous (Figure 1C), sometimes forming irregular clusters, rarely interwoven (Figure 1A) with variable tendencies for coiling (Figure 1C,D). Sheaths are colorless, very thin, visible after staining with Indian ink (Figure 1H). Trichomes uniseriate, isopolar, without false branching, constricted at the cross-walls, non-motile (Figure 1C–H). Vegetative cells are cylindrical with rounded ends, oval or barrel-shaped (3.3) 3.5–6.6  $\mu\text{m}$  long and 2.6–3.5  $\mu\text{m}$  wide, brown in color with smooth and finely granulated content. Apical cell rounded. Very slightly tapered terminal cells were sometimes observed. Heterocytes in terminal and intercalary positions, mostly solitary, rarely up to three in a row with yellow–green homogenous content (Figure 1C,E–H). Terminal heterocytes almost spherical to spherical (3.0) 3.2–5.0 (5.6)  $\mu\text{m}$  in diameter, and cylindrical with rounded ends to oblong 3.9–5.9  $\mu\text{m}$  long and (3.2) 3.4–4.0  $\mu\text{m}$  wide. Intercalary heterocytes cylindrical with rounded ends or cylindrical to oval (4.2) 4.4–7.0 (7.4)  $\mu\text{m}$  long and (2.8) 3.1–5.0 (5.7)  $\mu\text{m}$  wide or almost spherical to spherical 3.6–5.0 (5.7)  $\mu\text{m}$  in diameter. Akinetes develop in rows (Figure 1I,J). Fully developed akinetes appear spherical to oval, with dark green color, up to 12  $\mu\text{m}$  wide. Motile hormogonia with gas vesicles bearing terminal heterocytes were occasionally observed (Figure 1K).

**SEM observations:** SEM examination confirms the morphology of the trichomes (Figure 1B).

**TEM observations:** Cell ultrastructure is shown in Figure 2. Nucleoid region is scattered through the cytoplasm (Figure 2A–F). In this region, there are ribosomes, carboxysomes (Figure 2F) and storage inclusions, such as cyanophycin granules and polyphosphate bodies, appearing as black or electron transparent reserve spaces (Figure 2D). The thylakoidal system surrounds the nucleoid regions with the thylakoids arranged in small curved or whorled parallel groups (Figure 2C–F). Cell division proceeds by the formation of a septum, which is continuous with the peptidoglycan layer (Figure 2E). Plasmodesmata were also observed (Figure 2D).

**Etymology:** al.ka.li'phi.lum. N.L. n. alkali (from the Arabic word 'alqali', ashes of salt wort); N.L. adj. philus -a -um (from Gr. masc. n. philos, friend); N.L. neut. adj. alkaliphilum, friend of alkaline environments.

**Habitat:** free-living, planktic in alkaline brackish waters.

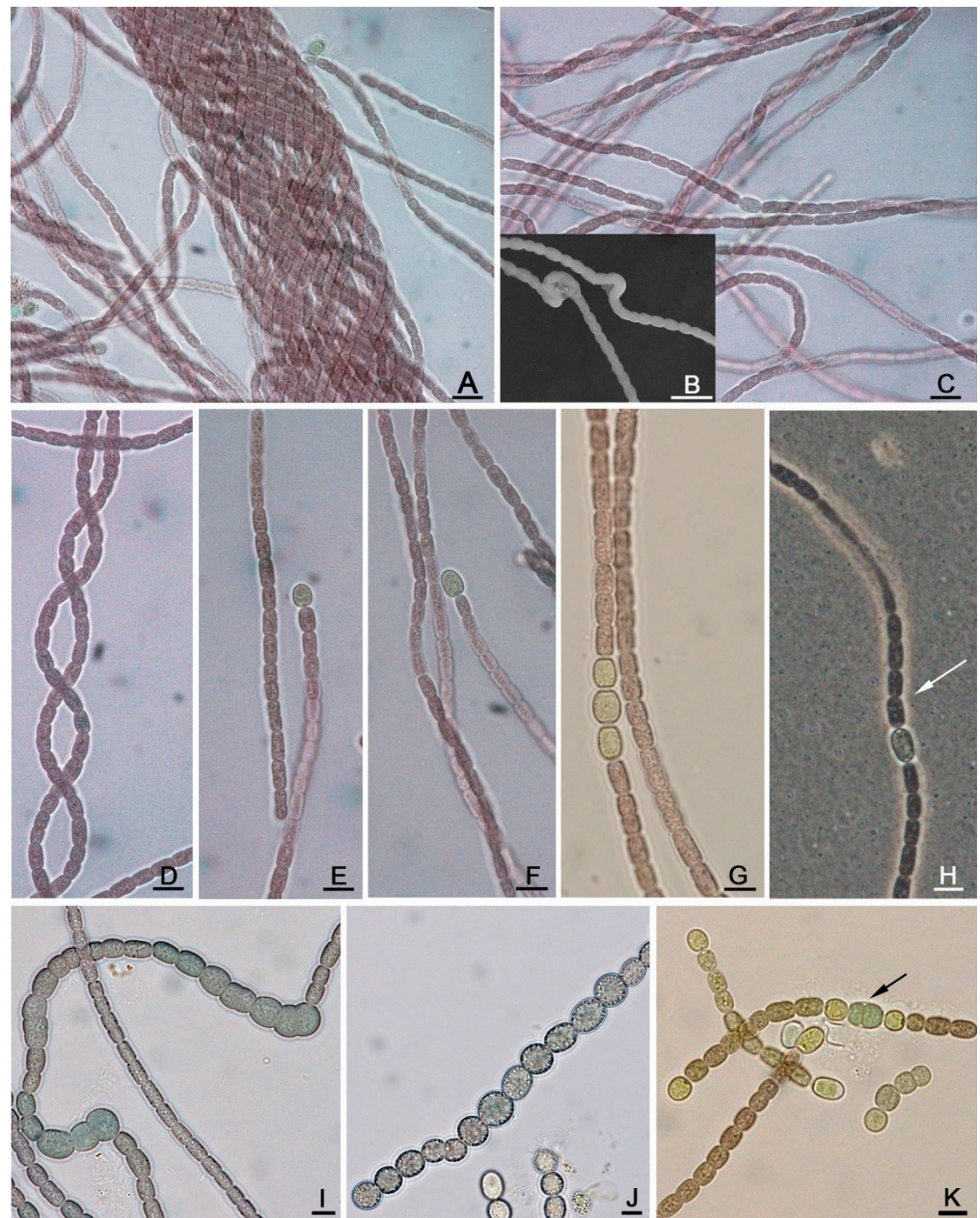


**Figure 1.** LM and SEM micrographs of *Aliinostoc alkaliphilum*. (A) Filaments of strain CENA513<sup>T</sup>. (B) Filament morphology of CENA513<sup>T</sup> as seen under SEM. (C) Filaments of CENA513<sup>T</sup> bearing solitary intercalary heterocyte. (D) A single coiled filament of CENA514. (E,F) Solitary heterocytes of variable size and shape at terminal positions in strains CENA514 and CENA524, respectively. (G) Filament of CENA513<sup>T</sup> bearing three adjacent heterocytes of variable size and shape at intercalary position. (H) Sheath (arrow) of CENA513<sup>T</sup> as seen after negative staining with India ink. (I) Early stage of akinete development in strain CENA524. (J) Fully developed akinetes in strain CENA524. (K) Akinete germination (arrow) and hormogonia bearing terminal heterocytes CENA514. Scale bars (A) = 5  $\mu\text{m}$ , (B) = 10  $\mu\text{m}$ , (C–K) = 5  $\mu\text{m}$ .

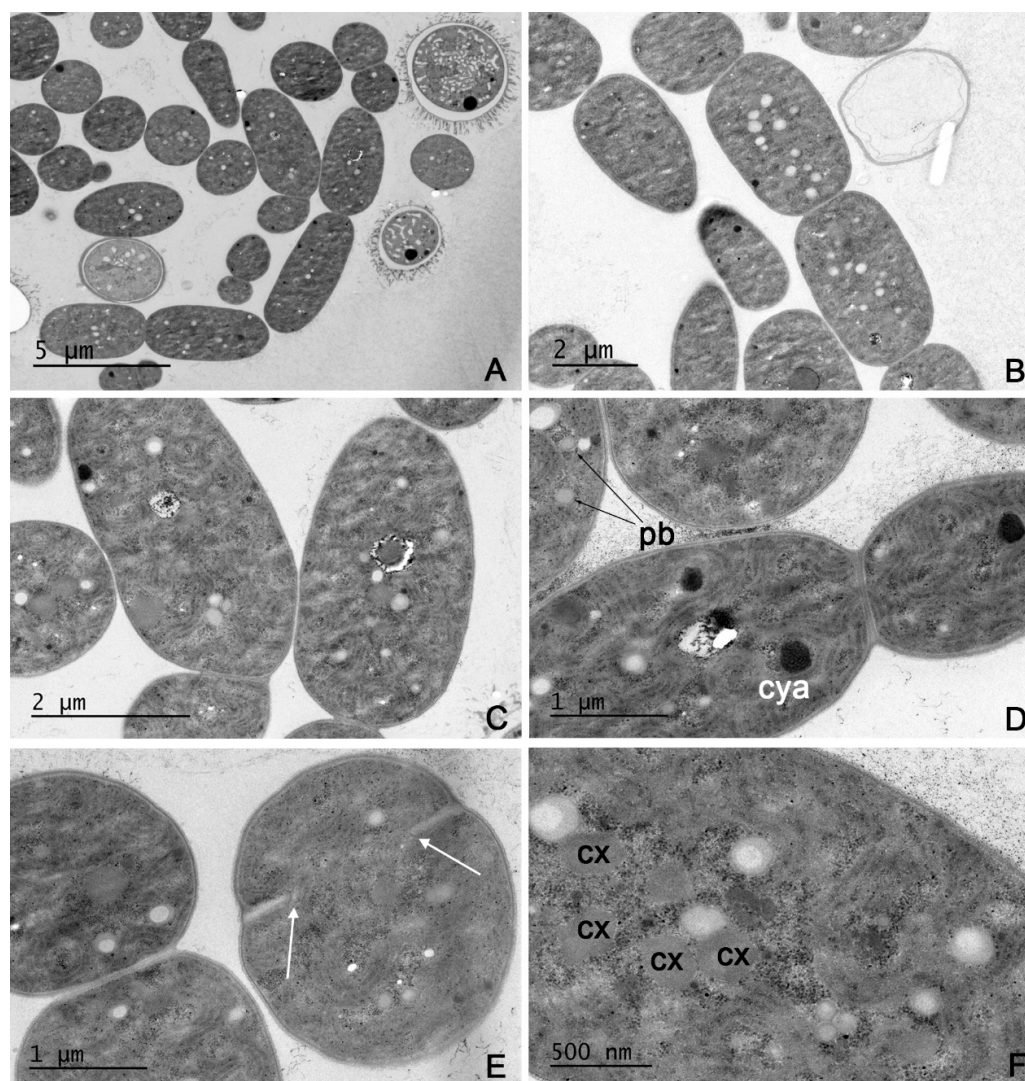


**Figure 2.** TEM micrographs of *Aliinostoc alkaliphilum* CENA513. (A–D) Longitudinal section of vegetative cells. Thylakoids are scattered throughout the cytoplasm forming curled bundles of parallelly arranged membranes. Polyphosphate bodies (pb) and cyanophycin granules (cya) are also observed. (E) Akinete germination and septum formation (arrows). (F) Carboxysomes (cx) seen as polyhedral bodies.

**Type locality:** Salina Verde (Coordinates; 19°28'13" S and 56°3'22" W), Pantanal wetland, Brazil.

**Holotype here designated:** Exsiccate accession number SP400047, deposited at “Maria Eneyda P. Kauffman Fidalgo” Herbarium of the Instituto de Pesquisas Ambientais, São Paulo state, Brazil.

**Type strain:** CENA513<sup>T</sup>.

*A. alkaliphilum* can be distinguished from the remaining *Aliinostoc* species based on its habitat preferences and morphological features observed under light microscope (Table S3). Unlike all other validly described *Aliinostoc* species (*A. morphoplasticum* NOS, *A. catenatum* SA24 and *A. magnakinatifex* SA18) that form macroscopic mats in slightly alkaline environments (pH 7–8) in India (*A. morphoplasticum* NOS) and Iran (*A. catenatum* SA24 and *A. magnakinatifex* SA18), *A. alkaliphilum* is a planktic species thriving in highly alkaline waters (pH 8.4–9.7) in Brazil. Furthermore, *A. alkaliphilum* is characterized by dark brown cells and the presence of two to three adjacent heterocysts, while the previously described *Aliinostoc* species were characterized by yellowish-brown colored cells (*A. morphoplasticum*

NOS) or blue-green colored cells (*A. catenatum* SA24 and *A. magnakinatifex* SA18) and solitary heterocytes. The spherical to oval akinete shape of *A. alkaliphilum* set this species apart from *A. morphoplasticum* NOS and *A. catenatum* SA24 which possess oblong and oval akinetes, respectively.

### 3.2. Phylogenetic Analyses and 16S-23S ITS Secondary Structures of *Aliinostoc*

A total of 231 taxa were used in the phylogenetic analysis. The 16S rRNA nucleotide sequences of the three studied strains, previously deposited in NCBI under the accession numbers KX458483 (CENA513), KX458484 (CENA514) and KX458485 (CENA524), were 1413 bp long and shared 99.56–99.83% sequence similarity with each other and 97.53–97.85% sequence similarity with the type strain of *Aliinostoc*, *A. morphoplasticum* NOS (Table S4). Both BI and ML analyses yielded nearly identical topologies and were mapped on the same phylogenetic tree (Figure 3). In both analyses, several distinct clades were supported by high bootstrap and posterior probability values. Similarly, genus *Aliinostoc* formed a well-supported monophyletic clade, which appeared to be more closely related to *Purpureonostoc* and other, morphologically distinct genera of Aphanizomenaceae and Nostocaceae (see Figure 3) than *Nostoc sensu stricto* clade. The same analyses showed that the three studied strains, CENA513<sup>T</sup>, CENA514 and CENA524, were firmly placed within the *Aliinostoc* clade.

Two ITS regions, containing either both or no tRNAs, were obtained from each studied strain. D1-D1' and box B regions from the non-tRNA containing operons of *A. alkaliphilum* strains were compared to the corresponding secondary structures of all known *Aliinostoc* (Figures 4 and 5 and Table 1). Secondary structures of D1 stem region and box B from tRNA-containing operons of *A. alkaliphilum* are presented in Figure S1, whereas a detailed description of all D1 helices and box B regions is presented in Table S5. For *Aliinostoc alkaliphilum*, D1-D1' helix was identical in all operons lacking tRNAs (Figure 4D) but had significant differences from the remaining *Aliinostoc* species in terms of length (Table 1), primary and secondary structures, except from the 6 bp-long basal stem (GACCUA-UAGGUC), which was common in all *Aliinostoc* species (Figure 4A–D). In detail, the D1 stem region of *A. alkaliphilum* is characterized by a 6 bp-long basal stem followed by a 5-residue right bulge, a 1-residue right bulge, a 3-residue asymmetrical internal loop and an 11-residue terminal hairpin (Figure 4D and Table S5). On the other hand, D1-D1' helices of *A. morphoplasticum* NOS and *A. catenatum* SA24 were characterized by the presence of a 6-residue basal stem followed by five internal loops and a 4 bp-long terminal hairpin (Figure 4A,B and Table S5). In contrast to *A. alkaliphilum*, the D1 helix of *A. magnakinatifex* SA18 is characterized by an 8-residue asymmetrical internal loop followed by a 2-residue left bulge, a 7-residue asymmetrical internal loop and 5-residue terminal hairpin (Table S5).

**Table 1.** Nucleotide sequence length of D1-D1' and box B regions of 16S-23S ITS of known *Aliinostoc* species.

Strain Name	D1-D1'	Box B
<i>Aliinostoc morphoplasticum</i> NOS	93	25
<i>Aliinostoc catenatum</i> SA24	93	26
<i>Aliinostoc magnakinatifex</i> SA18	60	33
<i>Aliinostoc alkaliphilum</i> (all three strains)	54	25

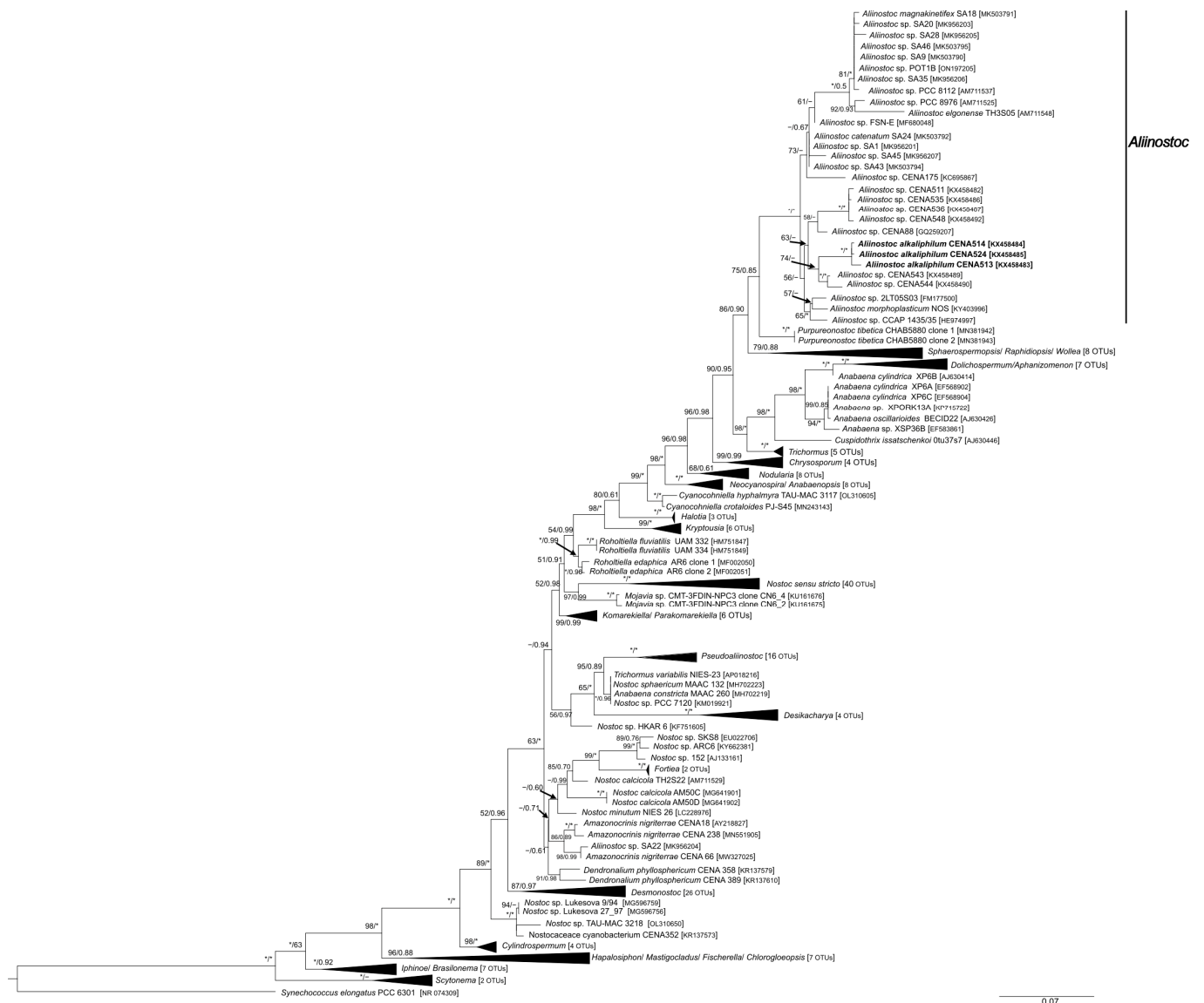


**Figure 3.** Phylogenetic relationships inferred from maximum likelihood analysis based on 16S rRNA sequences of *Aliinostoc* and related genera of Nostocales sensu Komarek et al. [13]. Sequences of *Aliinostoc alkaliphilum* CENA513<sup>T</sup>, 514 and 524 are shown in bold. Numbers on nodes correspond to bootstrap values ( $\geq 50\%$ ) and posterior probabilities ( $\geq 0.50$ ) obtained from maximum likelihood and Bayesian analyses, respectively. Asterisk (\*) represents posterior probability of 1.0 for Bayesian analysis and bootstrap values of 100% for maximum likelihood analysis. *Synechococcus elongatus* PCC 6301 was the designated outgroup. GenBank accession numbers of sequences are given in brackets. The scale corresponds to substitutions/site.

## D1-D1' helices

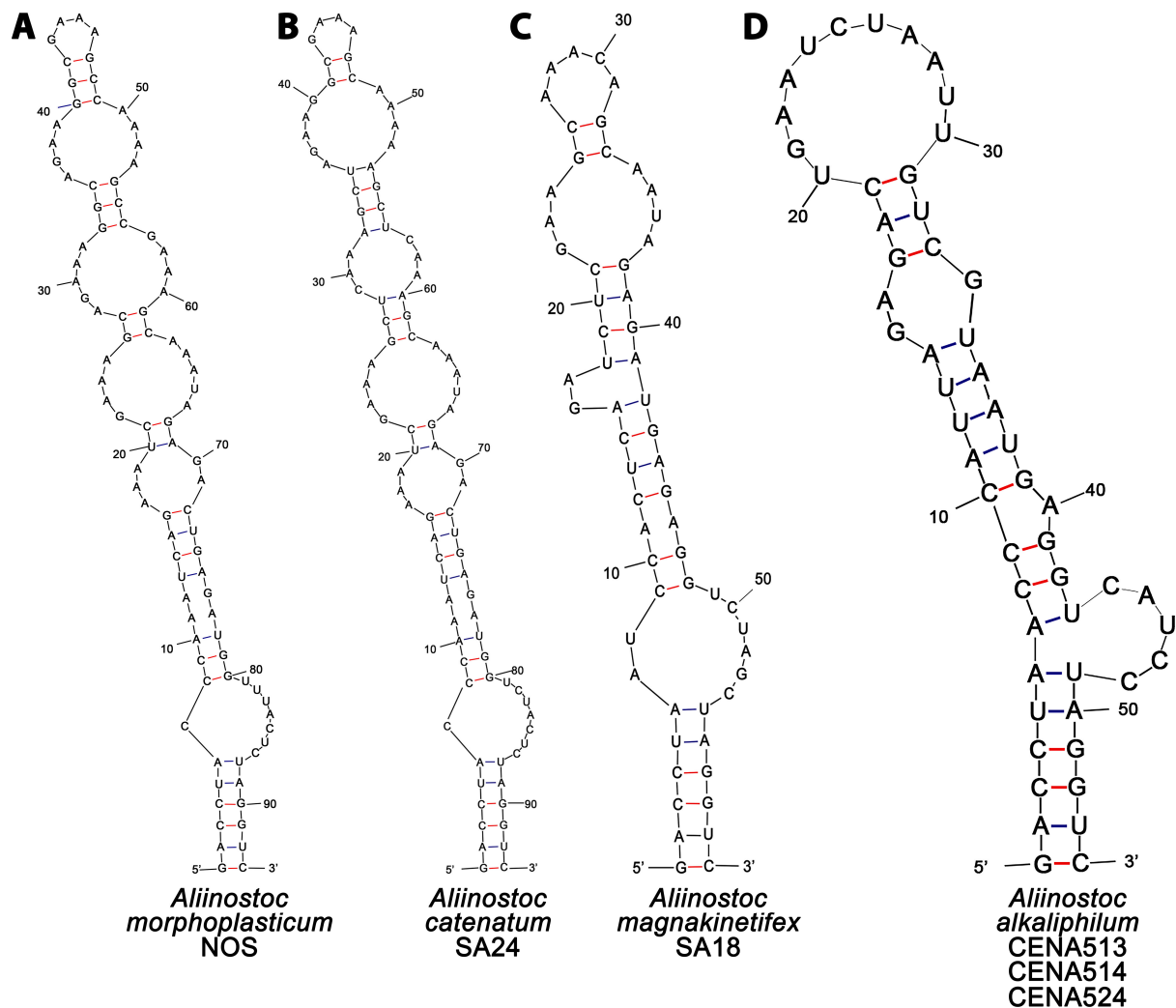


**Figure 4.** Hypothetical secondary structures of conserved D1-D1' region of the 16S-23S ITS regions of *Aliinostoc* species identified in operons lacking tRNA genes. (A) *Aliinostoc morphoplasticum* NOS (KY403996). (B) *A. catenatum* SA24 (MK503792). (C) *A. magnakinetifex* SA18 (MK503791). (D) *A. alkaliphilum* CENA513<sup>T</sup>, CENA514 and CENA524 (OK042917, OK042919 and OK042921, respectively).

The box B structures of all three *A. alkaliphilum* strains were identical to each other (Figure 5D) and structurally identical to *A. morphoplasticum* NOS (Figure 5A). Both *A. alkaliphilum* and *A. morphoplasticum* NOS box B folded structures were characterized by a 4 bp-long basal stem, followed by a 3-residue asymmetrical internal loop, a 5-residue stem region and a 4-residue terminal hairpin. The only differences observed between these two species were the presence of guanine (G) at position 9 of *A. alkaliphilum* instead of adenine (A) as in *A. morphoplasticum* NOS and the nucleotide sequence of their terminal hairpin (5'-GAAA-3' in *A. alkaliphilum* and 5'-AAUU-3' in *A. morphoplasticum* NOS). The box B regions of *A. catenatum* SA24 and *A. magnakinetifex* SA18 differ from *A. alkaliphilum* in respect to their sequence length (Table 1), primary and secondary structures. In detail, *A. catenatum* SA24 (Figure 5B) differs from *A. alkaliphilum* (Figure 5D) by having a 5 bp instead of a 4 bp-long basal stem followed by a 4-residue asymmetrical internal loop (3-residue in *A. alkaliphilum*) and a 4-residue stem region (5 bp-long stem region in *A. alkaliphilum*). Furthermore, the nucleotide sequence of the terminal hairpin in *A. catenatum* SA24 (5'-CGCU-3') is significantly different from *A. alkaliphilum* (5'-GAAA-3'). In the box B structure of *A. magnakinetifex* SA18 (Figure 5C), the 5-residue basal stem is followed by a 4-residue

asymmetrical internal loop, a 3-residue stem region, a 5-residue asymmetrical internal loop, a 2-residue stem region and a 4-residue terminal hairpin (5'-CGAG-3'). The presence of two internal loops as well as the nucleotide sequence of its terminal hairpin separates *A. magnakinatifex* SA18 from *A. alkaliphilum* and the remaining *Aliinostoc* species.

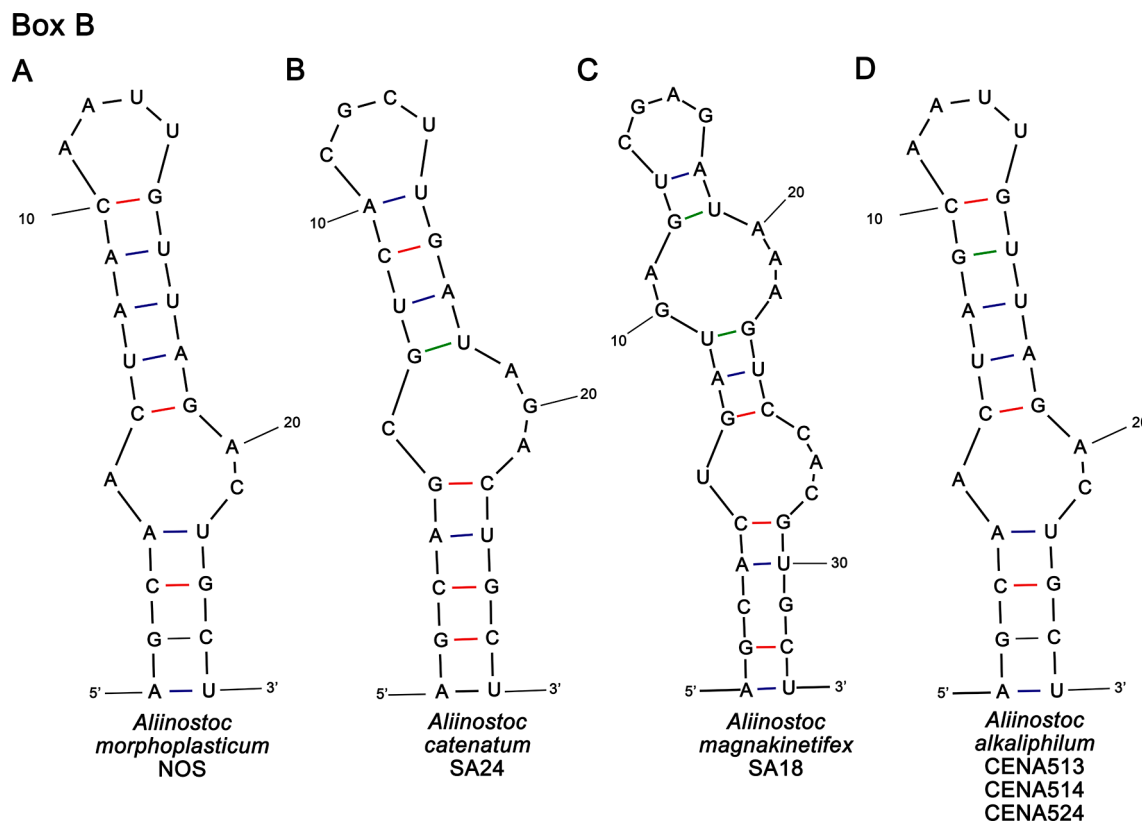


**Figure 5.** Hypothetical secondary structures of conserved box B helices of the 16S-23S ITS regions of *Aliinostoc* species identified in operons lacking tRNA genes. (A) *Aliinostoc morphoplasticum* NOS (KY403996). (B) *A. catenatum* SA24 (MK503792). (C) *A. magnakinatifex* SA18 (MK503791). (D) *A. alkaliphilum* CENA513<sup>T</sup>, CENA514 and CENA524 (OK042917, OK042919 and OK042921, respectively).

### 3.3. Antimicrobial Susceptibility Testing and Chemical Analysis

*Aliinostoc alkaliphilum* strains CENA513<sup>T</sup>, CENA514 and CENA524 inhibited the growth of *S. aureus*, *A. flavus* and *Mucor* sp. In addition, strain CENA513<sup>T</sup> also inhibited the growth of *B. cereus* (Table 2 and Figures S2 and S3). None of the studied *A. alkaliphilum* strains affected the growth of the remaining microbial strains, i.e., *E. faecium*, *M. luteus*, *P. aeruginosa*, *A. baumannii*, *E. aerogenes*, *S. enterica*, *C. albicans*, *C. krusei*, *C. parapsilosis* and *C. neoformans*. Antimicrobial tests carried out using HPLC fractions of CENA514 and 524 revealed the presence of antimicrobial metabolites in one HPLC fraction of CENA514 and one of CENA524. In both cases, the bioactive fractions exhibited bactericidal activity against *S. aureus*, fungicidal activity *A. flavus* and *Mucor* sp. and bacteriostatic activity against *B. cereus*. In strain CENA513<sup>T</sup>, bioactive metabolites were present in two HPLC fractions. One fraction exhibited the same bioactivities as in CENA514 and 524, whereas the second fraction exhibited bactericidal activity against *B. cereus* (Figures S4–S7).

LC-MS analysis of crude cyanobacterial extracts and bioactive fractions from all three strains was carried out to identify the dominant bioactive metabolite(s). The bioactive metabolite found in crude extracts of all three strains had  $m/z$  299.23 and its elemental composition was  $C_{16}H_{30}N_2O_3$ . As seen in Figure S9 and Table S6, mass spectra and product ion spectra of crude extracts from all three CENA strains matched well with the nocuolin A

reference material. Furthermore, strain CENA513<sup>T</sup> produced three to eleven times more nocuolin A (Figure 6) compared to the other two strains (Figure S8).

**Table 2.** Bioactivity screening results for *Aliinostoc alkaliphilum* strains.

Strain Name	Crude Extracts of <i>A. alkaliphilum</i> Strains			Controls	
	CENA513 <sup>T</sup>	CENA514	CENA524	Positive *	Negative **
<i>S. aureus</i>	+	+	+	+	–
<i>B. cereus</i>	+	–	–	+	–
<i>A. flavus</i>	+	+	+	+	–
<i>Mucor</i> sp.	+	+	+	+	–

Note: \* Positive controls: Bacteria: Kanamycin 1000 mg antibiotic disks; Fungi: sterile paper disks containing 50 µL of nystatin solution (1 mg mL<sup>-1</sup> dissolved in 70% MeOH). \*\* Negative control: sterile paper disks containing 300 µL of 100% MeOH.

Analysis of HPLC fractions showed that the total amount of nocuolin A present in each strain was only found in the bioactive fractions of CENA514 and 524 (99% and 97% of total amount of nocuolin A, respectively). Similarly, 97% of total amount of nocuolin A of CENA513<sup>T</sup> was found in one out of two bioactive fractions of CENA513<sup>T</sup> that inhibited the growth of *S. aureus*, *A. flavus* and *Mucor* sp. (Figures S10–S12).

The bioactive fraction of CENA513<sup>T</sup> that inhibited the growth of *B. cereus* contained three lysoglycerolipids (DGMG 16:1/0:0, SQMG 16:0/0:0, LPG 16:0/0:0) and five compounds with unresolved chemical structures.

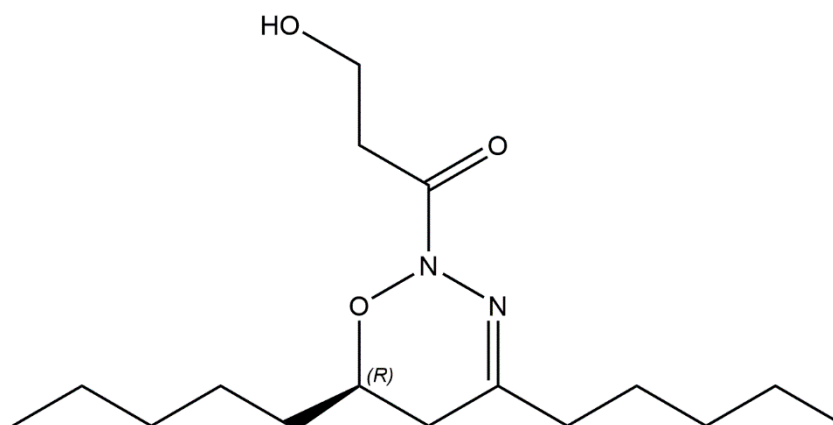


**Figure 6.** Chemical structure of the identified bioactive metabolite nocuolin A.

### 3.4. Taxonomic Distribution of Bioactive Metabolite-Producing *Nostoc*-like Strains

A total of 67 strains ascribed to *Nostoc* (including the three strains studied herein) produced 267 bioactive metabolites with a wide range of activities (Table S7). Nucleotide sequences of 16S rRNA gene were available for 43 strains (≈64%) and were included in our phylogenetic analysis. Sequencing data from *Nostoc* sp. BEA-0956 were also available but sequence was too short to be included in the analysis (≈800 bp). As seen in Figure 7 as well as Figure S13 and Table S7, only 17 out of 43 ‘*Nostoc*’ strains, producing 102 out of 267 bioactive compounds (≈38%), fall into the *Nostoc sensu stricto* clade. The remaining 26 strains (Figure 7 and Figure S13 and Table S7), which produce approximately 37% ( $n_{\text{comp}} = 98$ ) of the bioactive compounds that are attributed to *Nostoc*, are firmly placed within the recently established genera *Aliinostoc* ( $n_{\text{strains}} = 9$ ;  $n_{\text{comp}} = 30$ ), *Pseudoaliinostoc* ( $n_{\text{strains}} = 6$ ;  $n_{\text{comp}} = 36$ ), *Dendronalium* ( $n_{\text{strains}} = 1$ ;  $n_{\text{comp}} = 2$ ) and the well-known genus *Desmonostoc* ( $n_{\text{strains}} = 4$ ;  $n_{\text{comp}} = 6$ ). In addition, six strains belonging to five distinct genetic lineages within Nostocales (clades A–E; Figure S13) were responsible for the production of 24 bioactive metabolites, 15 of which were microcystin variants (Table S7 and Figure S13). Finally, 24 strains producing 67 compounds (≈25%), although assigned to *Nostoc* have

no morphological nor molecular data available to support this assignment, making their further study impossible (Table S7).

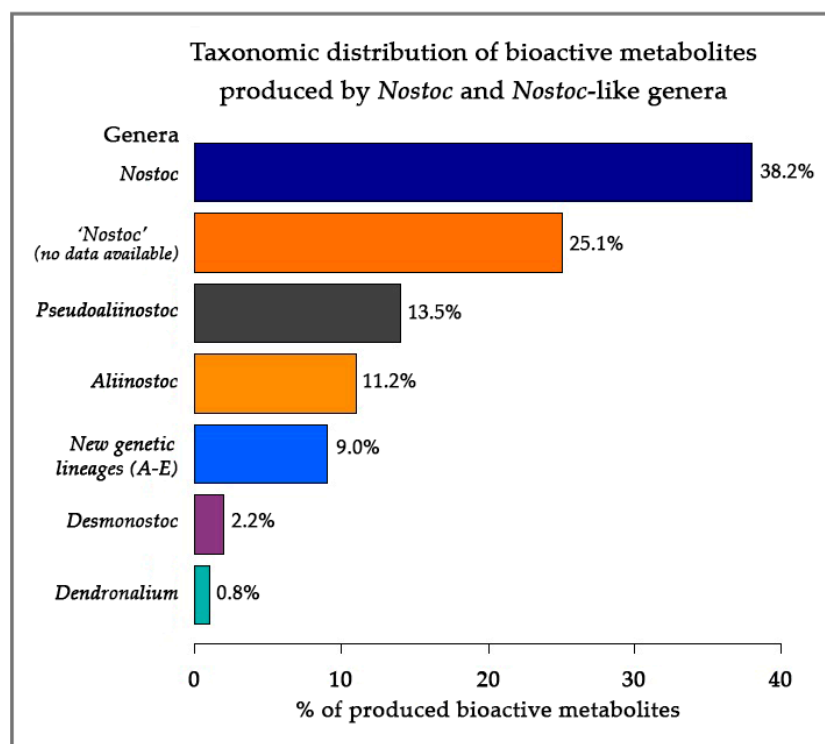


**Figure 7.** Taxonomic distribution of NP-producing strains assigned to *Nostoc* and *Nostoc*-like genera.

#### 4. Discussion

A new *Aliinostoc* species, *A. alkaliphilum*, exhibiting antibacterial and antifungal properties is described herein using a combination of cytomorphological, molecular and ecological criteria. Furthermore, the main bioactive metabolite identified in *A. alkaliphilum* is the recently described bioactive molecule nocuolin A [56]. Finally, this study shows that a great number of bioactive metabolite-producing strains, which are ascribed to *Nostoc*, belong to phylogenetically distant cyanobacterial lineages.

The genus *Aliinostoc*, with *A. morphoplasticum* NOS as the type strain, has been described from benthic rocks of a eutrophic pond in Sihora (Jabalpur, India) by Bagchi et al. [21]. Although *Aliinostoc* is morphologically indistinguishable from *Nostoc*, 16S rRNA phylogenetic analysis carried therein revealed a clear genetic separation of *Aliinostoc* from *Nostoc sensu stricto* and other nostocalean genera, thus allowing the establishment of this new genus. Differences observed in D1 stem and box B secondary structures of *Aliinostoc* and previously established genera further supported the abovementioned findings. Phylogenetic analyses of 16S rRNA also led Saraf et al. [57] and Kabirataj et al. [38] to the establishment of new *Aliinostoc* species (*A. soli*, *A. tiwarii* and *A. constrictum*, *A. catenatum*, *A. magnakinetifex*, respectively). However, recent studies of Lee et al. [24] supported the transfer of *A. soli*, *A. tiwarii* and *A. constrictum* to the new genus *Pseudoaliinostoc*, a genus that is morphologically similar but phylogenetically distant from *Aliinostoc* [24]. The 16S rRNA phylogenetic studies presented in our work are in line with the abovementioned findings.

##### 4.1. Molecular Evaluation

Herein, information deriving from 16S rRNA gene and ITS analysis in conjunction with light microscopy and ecological data support the placement of our strains under the recently described genus *Aliinostoc*. In detail, the three studied strains, i.e., CENA513<sup>T</sup>, CENA514 and CENA524, shared 97.53–97.85% 16S rRNA sequence similarity with the type strain of *Aliinostoc*, *A. morphoplasticum* NOS, which is higher than the 95.0% cut-off

point proposed by Stackebrandt and Goebel [58] for genus delimitation. Our strains shared 99.56–99.83% 16S rRNA sequence similarity with each other; these values are higher than the recommended threshold of 98.65% for bacterial species demarcation [59] and strongly suggest the establishment of a new *Aliinostoc* species.

It has been previously shown that the 16S-23S ITS region is more variable compared to 16S ribosomal gene [60,61] and a growing number of studies have used the information provided by 16S-23S ITS region as an additional tool in polyphasic approach studies of cyanobacterial strains. Specifically, the folded D1-D1', box B regions and, in some cases, V3 structures have been successfully used to support the establishment of new genera and species [21,38,62–67]. Herein, the differences observed between D1-D1' and box B regions of *A. alkaliphilum* and the remaining *Aliinostoc* further support the findings of 16S rRNA phylogenetic analysis. Unlike box B, which appears to be more conserved, the secondary structures of D1-D1' helices exhibit significant differences between different *Aliinostoc* species, except from *A. morphoplasticum* and *A. catenatum* that only have minor differences in their primary structure. High interspecies variability of the D1-D1' region has been previously observed in other genera such as *Potamolinea* [66], *Wilmottia* [68], *Ancylothrix* [65], *Macrochaete* [63] and many others.

The presence of multiple ribosomal operons containing one tRNA gene, both tRNA genes or no tRNA genes has been previously reported in many cyanobacterial taxa [44,69]. Unlike the previously described *Aliinostoc* species, which only have one operon lacking both tRNAs, the three *A. alkaliphilum* strains have two different operons. One operon contains both tRNAs (for isoleucine and alanine), whereas the second lacks both tRNAs. Although secondary structures of the tRNA-containing operons cannot be compared with the remaining *Aliinostoc* due to their lack of tRNAs, it is worth noting that the study of D1 stem in the tRNA-containing operons of our strains revealed the presence of two distinct patterns (see supplementary material). Interestingly one of the D1-D1' patterns observed in the tRNA-containing operons of *A. alkaliphilum* is structurally similar to the D1-D1' regions of *A. morphoplasticum* NOS and *A. catenatum* SA24. At the same time, the box B regions of the tRNA-containing operons of *A. alkaliphilum* were identical to the ones recovered from operons lacking tRNAs. Intraspecies variability of different ITS regions has been previously reported in different cyanobacterial taxa. For example, highly variable D1-D1', box B and V3 helices were observed in strains of *Ancylothrix terrestris* [65], whereas the D1-D1' and box B secondary structures of four *Koinonema perogatum* strains exhibited three and two distinct patterns, respectively [70]. Variable D1-D1', box B and V3 regions were also observed in several strains of *Scytonema hyalinum* [69].

#### 4.2. Morphology and Ecology of *Aliinostoc*

In addition to molecular data, macroscopic and microscopic characteristics as well as ecology further corroborate the establishment of *A. alkaliphilum*. Specifically, *A. magnakinatifex* SA18 and *A. catenatum* SA24 were isolated from slightly alkaline soil in Iran where they form greenish-blue colonies with tough mucilaginous texture and thick bluish-green macroscopic mats, respectively [38]. On the other hand, *A. morphoplasticum* NOS forms macroscopic mats on benthic rocks in eutrophic waters with slightly alkaline pH in Sihora, Jabalpur, India. The new species described herein (*A. alkaliphilum*) is planktic, does not form macroscopic mats in nature and was isolated from a Brazilian alkaline lake with pH levels that range between 8.4 and 9.7. In terms of morphology, cell width alone cannot be used for species discrimination in *Aliinostoc* since all species have overlapping minimum and maximum cell width dimensions. However, the darkbrown-colored cells of *A. alkaliphilum* and the presence of two to three adjacent heterocytes, separate our strains from the previously described *Aliinostoc* species that had cells with yellowish-brown (*A. morphoplasticum* NOS) or blue-green color (*A. catenatum* SA24 and *A. magnakinatifex* SA18) and solitary heterocytes. The spherical to oval akinete shape of *A. alkaliphilum* separates it from *A. morphoplasticum* NOS and *A. catenatum* SA24 that possess oblong and oval akinetes, respectively [21,38]. Lastly, *A. alkaliphilum* is characterized by motile hormogonia with

terminal heterocytes and gas vesicles. In a previous study, Bagchi and co-workers [21] reported that the presence of motile hormogonia characterizes all *Aliinostoc* strains and should be considered as the morphological autapomorphic diacritical character for the genus *Aliinostoc*. However, the only *Aliinostoc* species that share this characteristic are *A. morphoplasticum* and *A. alkaliphilum*. Based on these findings, this feature cannot be considered as an autapomorphic characteristic for this genus anymore.

#### 4.3. Bioactive Metabolites Produced by *Aliinostoc alkaliphilum*

As discussed by Genuário et al. [35], the number of studies dealing with the biodiversity of extremophilic cyanobacteria is limited, while studies exploring their bioactive potential are even scarcer. In this study, strains belonging to the extremophilic cyanobacterium *A. alkaliphilum* inhibited the growth of *S. aureus*, *Mucor* sp. and *Aspergillus flavus*. Chemical analysis of crude extracts revealed the presence of nocuolin A in different concentrations, which could explain the differences observed in inhibition zones produced by the three different CENA strains.

Nocuolin A is the first and thus far the only naturally occurring oxadiazine discovered from living organisms [56]. Specifically, nocuolin A was discovered by Voráčová and co-workers [56] while screening cyanobacterial strains for apoptosis inducers. Apart from anticancer activity, studies by González-Fuente et al. [71] revealed the antimicrobial potential of an unnamed compound, which is structurally identical to nocuolin A, as well as its isomers against pathogenic strains of *Nocardia*, *Tsarkamurella*, *Mycobacterium*, *Staphylococcus*, *Acinetobacter*, *Candida* and *Aspergillus*.

Although the bioactive fractions that inhibit the growth of *S. aureus*, *A. flavus* and *Mucor* sp. were characterized by impurities, the only common compound in all fractions was nocuolin A. The inhibitory activity of nocuolin A against *S. aureus* and *A. flavus* as well as the bacteriostatic activity of the compound against *B. cereus* is consistent with the previous findings of González-Fuente et al. [71], whereas the antifungal activity of nocuolin A against *Mucor* is reported here for the first time. No inhibitory activity was observed against *A. baumannii* and *C. parapsilosis*. These findings contradict the previous results of González-Fuente et al. [71] who showed that pure nocuolin A (100 µg per disk) inhibits the growth of *A. baumannii* (10–12 mm diameter of inhibition zone) and *C. parapsilosis*. These contradictory results could be explained by the different concentrations of nocuolin A in our cyanobacterial samples. However, purification of nocuolin A and additional antimicrobial susceptibility assays are required to confirm the abovementioned findings. To date, nocuolin A has been observed in heterocytous cyanobacteria belonging to *Nostoc*, *Dolichospermum*, *Anabaena*, *Nodularia* and *Trichormus* [56]. The discovery of nocuolin A in *A. alkaliphilum* expands the taxonomic distribution of this compound, which was thus far restricted to the abovementioned heterocyte-forming genera.

In addition to *S. aureus*, *Mucor* sp. and *Aspergillus flavus*, strain CENA513<sup>T</sup> exhibited anti-*Bacillus cereus* activity too. Bioactivity-guided fractionation of CENA513<sup>T</sup> crude extract revealed the presence of three lysoglycerolipids (DGMG 16:1/0:0, SQMG 16:0/0:0 and LPG 16:0/0:0) and five other unidentified molecules in fractions that inhibited the growth of this potential pathogen. The antimicrobial potential of SQMGs has been previously demonstrated [72,73] but there are no reports regarding the antibacterial potential of the remaining lysoglycerolipids. *B. cereus* is an opportunistic bacterial pathogen found in soil and food products [74]. Apart from the obvious pharmaceutical potential, the identification of metabolites that could specifically target *B. cereus* cells without affecting the quality of food products or having any cytotoxic effects may also have applications in the food industry. Therefore, further studies are required to isolate and characterize the interesting anti-*Bacillus cereus* compound(s).

#### 4.4. Taxonomic Distribution of Bioactive Metabolites

##### 4.4.1. Is genus *Nostoc* Rich in Bioactive Compounds?

Cyanobacteria are an attractive source of bioactive metabolites with biotechnological and pharmaceutical applications [4]. Interestingly, most of the bioactive metabolite-producing strains are ascribed to genera which are polyphyletic [6,9]. A recent example derives from the polyphyletic genus *Lyngbya*. According to Tidgewell and co-workers [75], 240 or 35% of marine cyanobacterial natural products derive from genus *Lyngbya*. Within *Lyngbya*, 183 out of 240 produced metabolites (76%) are attributed to *Lyngbya majuscula* [75]. This profound chemical prolificacy of *L. majuscula* morphotypes led Engene et al. [9] to a polyphasic approach study of *Lyngbya* populations aiming to provide a better understanding of the relationship between bioactive metabolite production and biological diversity of this chemically rich genus. Although all studied strains were morphologically similar to *Lyngbya*, phylogenetic analysis suggested that these *Lyngbya*-like strains fell outside the *Lyngbya sensu stricto* clade. This resulted in the establishment of the genus *Moorena* [8,76] followed by *Okeania* [11] and *Dapis* [10], which are nowadays considered responsible for the production of several bioactive metabolites previously assigned to *Lyngbya*. Similar to *Lyngbya*, the phylogenetic analysis presented herein revealed that several bioactive compounds ascribed to *Nostoc* belong to different cyanobacterial lineages. In fact, members of *Nostoc* produce less than 40% of the bioactive metabolites currently assigned to *Nostoc*. Most bioactive compound families such as microcystins, anabaenapeptins, microviridins, mycosporine-like amino acids and many others produced by *Nostoc* strains seem to be randomly distributed among different cyanobacterial lineages [5], but metabolites such as cryptophycins [77,78], merocyclophanes [79,80] and nosperin [81] appear to be exclusively produced by *Nostoc*. Considering that a total of 67 compounds are produced by strains with unclear taxonomic position, the possibility of identifying more 'true *Nostoc*' strains after the application of polyphasic approach studies is still possible. However, even if all these unclassified strains are assigned to *Nostoc*, the percentage of bioactive compounds produced by true *Nostoc* species is less than 64%.

##### 4.4.2. Bioactive Metabolites from *Nostoc*-like Genera

Based on data collected from CyanoMetDB [5] and our phylogenetic analysis, the recently established genera *Aliinostoc* and *Pseudoaliinostoc* produce 30 and 36 bioactive metabolites, respectively. Apart from nocuolin A produced by *A. alkaliphilum*, five more strains of the *Aliinostoc* clade produce 29 functionally and structurally diverse bioactive metabolites. These include *Aliinostoc* spp. CENA535 and CENA548 which produce the toxic lipopeptides puwainaphycins [82], the microcystin-producing *Aliinostoc* sp. strain CENA88 [83] and *Aliinostoc* sp. CENA175, which produces volatile compounds [84]. The abovementioned metabolites are produced by other cyanobacterial genera too [29]. The production of the trypsin inhibitors nostosins identified from *Aliinostoc* sp. strain FSN-E [27] and pseudospumigins, a new family of linear tetrapeptides that show protease inhibitory activity, reported from *Aliinostoc* sp. CENA543 [85], is thus far restricted to *Aliinostoc*. In addition to pseudospumigins, Jokela and co-workers [85] also report that *Aliinostoc* sp. CENA543 is the first free-living strain that produces very large amounts of the hepatotoxic metabolite nodularin-R. Furthermore, studies by Shishido et al. [86] revealed the production of new and known variants of namalides and anabaenapeptins by *Aliinostoc* sp. CENA543. The production of natural products in *Pseudoaliinostoc* is limited to [7.7] paracyclophanes, a family of aromatic polyketides exhibiting a broad spectrum of bioactivities ranging from antimicrobial to cytotoxic activities [87–91]. Specifically, *Pseudoaliinostoc* strains CAVN2, CAVN10 and UIC 10274 are the only known producers of carbamidocyclophanes [87,89,92,93], whereas ribocyclophanes have only been reported from *Pseudoaliinostoc* spp. UIC 10366 and UIC 10279 [90]. Lastly, *Pseudoaliinostoc* sp. UIC 10022A together with *Cylindrospermum licheniforme* and *Cylindrospermum stagnale* are the only known producers of cylindrocyclophanes [88,91,94,95]. The remaining groups of [7.7] paracyclophanes, i.e., merocyclophanes and nostocyclophanes, are produced by members of *Nostoc*, i.e., *Nostoc* spp.

UIC 10100 and UIC 10062 [79,80] and *Nostoc linckia* UTEX B1932, respectively [94,96,97]; the latter species has been transferred to the genus *Desmonostoc*. According to our phylogenetic analysis, muscoride A and B as well as deprenylmuscoride A and B [98,99] are produced by members of *Desmonostoc*. Furthermore, the production of these alkaloids together with muscotoxins produced by *D. muscorum* CCALA 125 [100] appears to be restricted to *Desmonostoc*. Lastly, the bioactive metabolites produced by *Dendronalium* and the remaining lineages A–E include anabaenapeptins and mycosporine-like amino acids which, as mentioned earlier, are widely distributed among cyanobacteria. Taking into consideration the above-mentioned findings, screening *Aliinostoc*, *Pseudoaliinostoc* as well as *Desmonostoc* strains for antimicrobial and/or anticancer substances may lead to the discovery of potentially new bioactive metabolites with potentially interesting biomedical and/or biotechnological applications in these relatively new cyanobacterial genera.

## 5. Conclusions

The new species *Aliinostoc alkaliphilum* from Salina Verde (Pantanal, Brazil) exhibiting antibacterial and antifungal properties is described in this study using a polyphasic approach. The identification of the bioactive metabolite nocuolin A in *Aliinostoc alkaliphilum* represents the first report of this metabolite in *Aliinostoc*. Furthermore, the utilization of all 16S rRNA sequencing data of bioactive metabolite-producing strains assigned to *Nostoc* contributed to a better understanding of the biodiversity and production of bioactive metabolites in this polyphyletic genus and other *Nostoc*-like genera. Results obtained herein also highlight the importance of polyphasic taxonomic studies in natural product discovery efforts.

**Supplementary Materials:** The following supporting information can be downloaded at: <https://www.mdpi.com/article/10.3390/w14162470/s1>, Figure S1: D1 stem region in *A. alkaliphilum* strains in tRNA-containing operons (A–B) and operons without tRNA (C). A: CENA513 and CENA514 (OK042916 and OK042918, respectively); B: *A. alkaliphilum* CENA524 (OK042920); C: *A. alkaliphilum* CENA513, CENA514 and CENA524 (OK042917, OK042919 and OK042921, respectively). Figure S2: Antibacterial susceptibility tests performed using crude cyanobacterial extracts. The amount of sample per disk was equivalent to 30 mg of freeze-dried biomass. (a–b) *Staphylococcus aureus* HAMBI 66. (c–d) *Bacillus cereus* HAMBI 1881. Note the bacteriostatic activity of CENA514 and 524 on *B. cereus* in contrast to bactericidal activity of CENA513 on the same pathogen. pos: positive control (Kanamycin 1000 µg per disk). neg: negative control (300 µL of 100% MeOH per disk). Disk diameter = 6 mm. Figure S3: Antifungal activity of *Aliinostoc alkaliphilum*. CENA513 (left), CENA514 (middle), CENA524 (right) on *Aspergillus flavus* HAMBI 829 (a–c) and *Mucor* sp. HAMBI 831 (d–f). The amount of sample per disk was equivalent to 30 mg of freeze-dried biomass. Zones of inhibition in CENA513 are clearly larger compared to CENA514 and CENA524. Disk diameter = 6 mm. Figure S4: Antimicrobial susceptibility tests performed using HPLC fractions and crude extract of *Aliinostoc alkaliphilum* CENA513 (a–c), CENA514 (d–f) and CENA524 (g–i) against *S. aureus* HAMBI 66. The concentration of metabolites in both HPLC fractions and crude extract corresponds to 30 mg of freeze-dried biomass. Numbers on disks correspond to HPLC fractions of CENA513, CENA514 and CENA524. Note that HPLC fraction 3 of CENA513 is present in figures a and b for comparison reasons. cr: crude extract. pos: positive control (kanamycin 1000 µg per disk). neg: negative control (300 µL of 100% MeOH per disk). Disk diameter = 6 mm. Figure S5: Antimicrobial susceptibility tests performed using HPLC fractions of *Aliinostoc alkaliphilum*. CENA513 (a,b) against *B. cereus* HAMBI 1881. Note the bactericidal activity of HPLC fraction 513#2 and bacteriostatic activity of HPLC fractions 513#3 and 513#4 on *B. cereus*. Crude extract (cr) was also used as a positive control. The concentration of metabolites in both HPLC fractions and crude extract corresponds to 30 mg of freeze-dried biomass. 1–4: HPLC fractions. pos: positive control (kanamycin 1000 µg per disk). neg: negative control (300 µL of 100% MeOH per disk). Disk diameter = 6 mm. Figure S6: Antifungal susceptibility tests performed using HPLC fractions and crude extract of *Aliinostoc alkaliphilum* CENA513 (a–c), CENA514 (d–f) and CENA524 (g–i) against *Mucor* sp. HAMBI 831. The concentration of metabolites in both HPLC fractions and crude extract corresponds to 10 mg of freeze-dried biomass. (c) Positive and negative controls. Numbers correspond to HPLC fractions. cr: crude extract. pos: positive control [50 µL of nystatin solution (1 mg mL<sup>-1</sup>)]. neg: negative control (300 µL of 100% MeOH per

disk). Disk diameter = 6 mm. Figure S7: Antifungal susceptibility tests performed using HPLC fractions and crude extract of *Aliinostoc alkaliphilum* CENA513 (a–c), CENA514 (d–f) and CENA524 (g–i) against *Aspergillus flavus*. HAMB1 829. The concentration of metabolites in both HPLC fractions and crude extract corresponds to 10 mg of freeze-dried biomass. (c) Positive and negative controls. Numbers correspond to HPLC fractions. cr: crude extract. pos: positive control [50  $\mu\text{L}$  of nystatin solution (1 mg  $\text{mL}^{-1}$ )]. neg: negative control (300  $\mu\text{L}$  of 100% MeOH per disk). Disk diameter = 6 mm. Figure S8: Total ion current (black) and extracted ion ( $m/z$  299.23; red) chromatograms (EIC) of CENA513, 514 and 524 strain crude extracts. Retention time in black font color and EIC areas in red font color. Figure S9: Mass spectra (A–C) of EIC peaks presented in Figure S8 and product ion spectra from  $m/z$  299.23 (E–G) of CENA513, 514 and 524 extracts and nocuolin A reference spectra (D, H) by Voráčová et al. [60]. Figure S10: Total ion chromatograms (TIC) and extracted ion  $m/z$  299.23 (protonated nocuolin A) chromatograms from *Aliinostoc alkaliphilum* CENA513 extract fractionated into 4 fractions by liquid chromatography. Peaks (TIC) eluting after 4.2 min are similarly present in all fractions and hence represent irrelevant compounds causing no bioactivity., Figure S11: Total ion chromatograms (TIC) and extracted ion  $m/z$  299.23 (protonated nocuolin A) chromatograms from *Aliinostoc alkaliphilum* CENA514 extract fractionated into 5 fractions by liquid chromatography. Figure S12: Total ion chromatograms (TIC) and extracted ion  $m/z$  299.23 (protonated nocuolin A) chromatograms from *Aliinostoc alkaliphilum*. CENA524 extract fractionated into 8 fractions by liquid chromatography. Figure S13: Phylogenetic relationships inferred from maximum likelihood analysis based on 16S rRNA sequences of *Aliinostoc* and related genera of Nostocales sensu Komarek et al. [13]. Clades hosting NP-producing strains (red font color) are shown in different font colors. All bioactive compounds produced by each strain are also shown. Numbers on nodes correspond to bootstrap values ( $\geq 50\%$ ) and posterior probabilities ( $\geq 0.50$ ) obtained from maximum likelihood and Bayesian analyses, respectively. Asterisk (\*) represents posterior probability of 1.0 for Bayesian analysis and bootstrap values of 100% for maximum likelihood analysis. *Synechococcus elongatus* PCC 6301 was the designated outgroup. GenBank accession numbers of sequences are given in brackets. The scale corresponds to substitutions/site. Table S1: Bacterial and fungal strains used in this study. Growth temperature and agar-solidified growth media used for strain propagation and disk diffusion assays are also presented. MH: Mueller–Hinton; MH-GMB: Mueller–Hinton with 2% glucose and 0.5  $\mu\text{g mL}^{-1}$  methylene blue; PDA: Potato Dextrose Agar. All bacterial and yeast strains were incubated overnight. Strains of filamentous fungi were incubated for 3 days. Table S2: Taxa included in the phylogenetic analyses and references for bioactive metabolite-producing strains. Table S3: Morphological comparison and habitat preferences of all known *Aliinostoc* species. Table S4: Comparison of the 16S rRNA gene sequence identity among *Aliinostoc* species and other Nostoclean taxa. Similarity =  $100 * [1 - (p\text{-distance})]$ . Table S5: Detailed description of the ITS secondary structures of *Aliinostoc* species. Table S6: Nocuolin A specific ion  $m/z$  values and formulas by Voráčová et al. [60] and difference ( $\Delta$ ) compared to calculated (Calc) values from MS spectra of CENA513, 514 and 524 strains. Mass of ions 14 and 16 were inaccurate but accurate in product ion spectra from  $m/z$  299.23. Table S7. Bioactive metabolite-producing strains and their GenBank accession numbers.

**Author Contributions:** Conceptualization, M.C. and K.S.; methodology, M.C., M.W., A.E.-A. and L.S.; validation, M.C., M.W. and J.J.; formal analysis, M.C., M.W. and J.J.; investigation, M.C.; resources, K.S., A.E.-A. and M.d.F.F.; data curation, M.C., M.W. and J.J.; writing—original draft preparation, M.C.; writing—review and editing, M.C., M.W., J.J., A.E.-A., M.d.F.F. and K.S.; visualization, M.C. and J.J.; supervision, J.J., A.E.-A. and K.S.; project administration, K.S.; funding acquisition, K.S. All authors have read and agreed to the published version of the manuscript.

**Funding:** This work was supported by a Jane and Aatos Erkkö Foundation (Finland) grant to K.S. and Sao Paulo Research Foundation (FAPESP #2016/14227–5) grant to M.d.F.F. M.C. is supported by a scholarship provided by the Vilho, Yrjö and Kalle Väisälä Foundation of the Finnish Academy of Science and Letters. Open access funding provided by University of Helsinki.

**Institutional Review Board Statement:** Not applicable.

**Data Availability Statement:** All nucleotide sequences used in this study are available from NCBI. For accession numbers see supplementary material.

**Acknowledgments:** The authors would like to thank the personnel of Electron Microscopy Unit of the Institute of Biotechnology, University of Helsinki for providing laboratory facilities and their help with sample preparation for Transmission Electron Microscopy.

**Conflicts of Interest:** The authors declare no conflict of interest.

## References

1. Whitton, B.A.; Potts, M. Introduction to the Cyanobacteria. In *Ecology of Cyanobacteria II*; Whitton, B.A., Ed.; Springer: Dordrecht, The Netherlands, 2012; pp. 1–13.
2. Swain, S.S.; Paidesetty, S.K.; Padhy, R.N. Antibacterial, antifungal and antimycobacterial compounds from cyanobacteria. *Biomed. Pharmacother.* **2017**, *90*, 760–776. [[CrossRef](#)] [[PubMed](#)]
3. Mazard, S.; Penesyan, A.; Ostrowski, M.; Paulsen, I.T.; Egan, S. Tiny microbes with a big impact: The role of cyanobacteria and their metabolites in shaping our future. *Mar. Drugs* **2016**, *14*, 97. [[CrossRef](#)] [[PubMed](#)]
4. Singh, R.K.; Tiwari, S.P.; Rai, A.K.; Mohapatra, T.M. Cyanobacteria: An Emerging source for drug discovery. *J. Antibiot.* **2011**, *64*, 401–412. [[CrossRef](#)] [[PubMed](#)]
5. Jones, M.R.; Pinto, E.; Torres, M.A.; Dörr, F.; Mazur-Marzec, H.; Szubert, K.; Tartaglione, L.; Dell’Aversano, C.; Miles, C.O.; Beach, D.G.; et al. CyanoMetDB, a comprehensive public database of secondary metabolites from cyanobacteria. *Water Res.* **2021**, *196*, 1–12. [[CrossRef](#)]
6. Leão, P.N.; Engene, N.; Antunes, A.; Gerwick, W.H.; Vasconcelos, V. The chemical ecology of cyanobacteria. *Nat. Prod. Rep.* **2012**, *29*, 372–391. [[CrossRef](#)]
7. Engene, N.; Gunasekera, S.P.; Gerwick, W.H.; Paul, V.J. Phylogenetic inferences reveal a large extent of novel biodiversity in chemically rich tropical marine cyanobacteria. *Appl. Environ. Microbiol.* **2013**, *79*, 1882–1888. [[CrossRef](#)]
8. Engene, N.; Rottacker, E.C.; Kaštovský, J.; Byrum, T.; Choi, H.; Ellisman, M.H.; Komárek, J.; Gerwick, W.H. *Moorea producens* gen. nov., sp. nov. and *Moorea bouillonii* comb. nov., tropical marine cyanobacteria rich in bioactive secondary metabolites. *Int. J. Syst. Evol. Microbiol.* **2012**, *62*, 1171–1178. [[CrossRef](#)]
9. Engene, N.; Choi, H.; Esquenazi, E.; Rottacker, E.C.; Ellisman, M.H.; Dorrestein, P.C.; Gerwick, W.H. Underestimated biodiversity as a major explanation for the perceived rich secondary metabolite capacity of the cyanobacterial genus *Lyngbya*. *Environ. Microbiol.* **2011**, *13*, 1601–1610. [[CrossRef](#)]
10. Engene, N.; Tronholm, A.; Paul, V.J. Uncovering cryptic diversity of *Lyngbya*: The new tropical marine cyanobacterial genus *Dapis* (Oscillatoriales). *J. Phycol.* **2018**, *54*, 435–446. [[CrossRef](#)]
11. Engene, N.; Paul, V.J.; Byrum, T.; Gerwick, W.H.; Thor, A.; Ellisman, M.H. Five chemically rich species of tropical marine cyanobacteria of the genus *Okeania* gen. nov. (Oscillatoriales, Cyanoprokaryota). *J. Phycol.* **2013**, *49*, 1095–1106. [[CrossRef](#)]
12. Engene, N.; Tronholm, A.; Salvador-Reyes, L.A.; Luesch, H.; Paul, V.J. *Caldora penicillata* gen. nov., comb. nov. (Cyanobacteria), a pantropical marine species with biomedical relevance. *J. Phycol.* **2015**, *51*, 670–681. [[CrossRef](#)]
13. Komárek, J.; Kaštovský, J.; Mareš, J.; Johansen, J.R. Taxonomic classification of Cyanoprokaryotes (cyanobacterial genera) 2014, using a polyphasic approach. *Preslia* **2014**, *86*, 295–335.
14. Hoffmann, L.; Komárek, J.; Kaštovský, J. System of Cyanoprokaryotes (Cyanobacteria)—State in 2004. *Arch. Hydrobiol. Suppl. Algal. Stud.* **2005**, *117*, 95–115. [[CrossRef](#)]
15. Johansen, J.R.; Casamatta, D.A. Recognizing cyanobacterial diversity through adoption of a new species paradigm. *Arch. Hydrobiol. Suppl. Algal. Stud.* **2005**, *117*, 71–93. [[CrossRef](#)]
16. Řeháková, K.; Johansen, J.R.; Casamatta, D.A.; Xuesong, L.; Vincent, J. Morphological and molecular characterization of selected desert soil cyanobacteria: Three species new to science including *Mojavia pulchra* gen. et sp. nov. *Phycologia* **2007**, *46*, 481–502. [[CrossRef](#)]
17. Saraf, A.G.; Dawda, H.G.; Singh, P. *Desikacharya* gen. nov., a phylogenetically distinct genus of cyanobacteria along with the description of two new species, *Desikacharya nostocoides* sp. nov. and *Desikacharya soli* sp. nov., and reclassification of *Nostoc thermotolerans* to *Desikacharya thermotolerans* comb. nov. *Int. J. Syst. Evol. Microbiol.* **2019**, *69*, 307–315.
18. Hrouzek, P.; Lukešová, A.; Mareš, J.; Ventura, S. Description of the cyanobacterial genus *Desmonostoc* gen. nov. including *D. muscorum* comb. nov. as a distinct, phylogenetically coherent taxon related to the genus *Nostoc*. *Fottea* **2013**, *13*, 201–213. [[CrossRef](#)]
19. Genuário, D.; Vaz, M.; Hentschke, G.; Sant’Anna, C.; Fiore, M. *Halotia* gen. nov., a phylogenetically and physiologically coherent cyanobacterial genus isolated from marine coastal environments. *Int. J. Syst. Evol. Microbiol.* **2015**, *65*, 633–675. [[CrossRef](#)]
20. Hentschke, G.S.; Johansen, J.R.; Pietrasiak, N.; Rigonato, J.; Fiore, M.F.; Sant’Anna, C.L. *Komarekiella atlantica* gen. et sp. nov. (Nostocaceae, Cyanobacteria): A new subaerial taxon from the atlantic rainforest and Kauai, Hawaii. *Fottea* **2017**, *17*, 178–190. [[CrossRef](#)]
21. Bagchi, S.N.; Dubey, N.; Singh, P. Phylogenetically distant clade of nostoc-like taxa with the description of *Aliinostoc* gen. nov. and *Aliinostoc morphoplacticum* sp. nov. *Int. J. Syst. Evol. Microbiol.* **2017**, *67*, 3329–3338. [[CrossRef](#)]
22. Cai, F.; Li, X.; Yang, Y.; Jia, N.; Huo, D.; Li, R. *Compactonostoc shennongjiaensis* gen. & sp. nov. (Nostocales, Cyanobacteria) from a wet rocky wall in china. *Phycologia* **2019**, *58*, 200–210.
23. Soares, F.; Ramos, V.; Trovão, J.; Cardoso, S.M.; Tiago, I.; Portugal, A. *Parakomarekiella sesnandensis* gen. et sp. nov. (Nostocales, Cyanobacteria) Isolated from the Old Cathedral of Coimbra, Portugal (UNESCO World Heritage Site). *Eur. J. Phycol.* **2021**, *56*, 301–315. [[CrossRef](#)]
24. Lee, N.J.; Bang, S.-D.; Kim, T.; Ki, J.S.; Lee, O.M. *Pseudoaliinostoc sejongensis* gen. & sp. nov. (Nostocales, Cyanobacteria) from floodplain soil of the geum river in korea based on polyphasic approach. *Phytotaxa* **2021**, *479*, 55–70.

25. Sivonen, K. Cyanobacterial Toxins. In *Encyclopedia of Microbiology*; Schaechter, M., Ed.; Elsevier: Oxford, UK, 2009; pp. 290–307.
26. Chorus, I.; Welker, M. *Toxic Cyanobacteria in Water: A Guide to Their Public Health Consequences, Monitoring and Management*, 2nd ed.; Chorus, I., Welker, M., Eds.; CRC Press, on Behalf of the World Health Organization: Geneva, Switzerland, 2021.
27. Liu, L.; Jokela, J.; Wahlsten, M.; Nowruzi, B.; Permi, P.; Zhang, Y.Z.; Xhaard, H.; Fewer, D.P.; Sivonen, K. Nostosins, trypsin inhibitors isolated from the terrestrial cyanobacterium *Nostoc* sp. strain FSN. *J. Nat. Prod.* **2014**, *77*, 1784–1790. [[CrossRef](#)]
28. Humisto, A.; Herfindal, L.; Jokela, J.; Karkman, A.; Bjørnstad, R.; Choudhury, R.R.; Sivonen, K. Cyanobacteria as a source for novel anti-leukemic compounds. *Curr. Pharm. Biotechnol.* **2016**, *17*, 78–91. [[CrossRef](#)] [[PubMed](#)]
29. Dittmann, E.; Gugger, M.; Sivonen, K.; Fewer, D.P. Natural product biosynthetic diversity and comparative genomics of the cyanobacteria. *Trends Microbiol.* **2015**, *23*, 642–652. [[CrossRef](#)] [[PubMed](#)]
30. Nowruzi, B.; Haghghat, S.; Fahimi, H.; Mohammadi, E. *Nostoc* cyanobacteria species: A new and rich source of novel bioactive compounds with pharmaceutical potential. *J. Pharm. Health Serv. Res.* **2018**, *9*, 5–12. [[CrossRef](#)]
31. Thuan, N.H.; An, T.T.; Shrestha, A.; Canh, N.X.; Sohng, J.K.; Dhakal, D. Recent advances in exploration and biotechnological production of bioactive compounds in three cyanobacterial genera: *Nostoc*, *Lyngbya*, and *Microcystis*. *Front. Chem.* **2019**, *7*, 1–33. [[CrossRef](#)]
32. Grant, W.D. Alkaline systems and biodiversity. In *Extremophiles*; Gerday, C., Glansdorff, N., Eds.; Eolss Publishers: Oxford, UK, 2006; pp. 21–38.
33. Sorokin, D.Y.; Berben, T.; Melton, E.D.; Overmars, L.; Vavourakis, C.D.; Muyzer, G. Microbial diversity and biogeochemical cycling in soda lakes. *Extremophiles* **2014**, *18*, 791–809. [[CrossRef](#)]
34. Andreote, A.P.D.; Dini-Andreote, F.; Rigonato, J.; Machineski, G.S.; Souza, B.C.E.; Barbiero, L.; Rezende-Filho, A.T.; Fiore, M.F. Contrasting the genetic patterns of microbial communities in soda lakes with and without cyanobacterial bloom. *Front. Microbiol.* **2018**, *9*, 1–13. [[CrossRef](#)]
35. Genuário, D.B.; Vaz, M.G.M.V.; Santos, S.N.; Kavamura, V.N.; Melo, I.S. Cyanobacteria from Brazilian Extreme environments: Toward functional exploitation. In *Microbial Diversity in the Genomic Era*; Das, S., Dash, H.R., Eds.; Academic Press: London, UK, 2019; pp. 265–284.
36. Andreote, A.P.D.; Vaz, M.G.M.V.; Genuário, D.B.; Barbiero, L.; Rezende-Filho, A.T.; Fiore, M.F. Nonheterocytous cyanobacteria from Brazilian saline-alkaline lakes. *J. Phycol.* **2014**, *50*, 675–684. [[CrossRef](#)]
37. Genuário, D.B.; Andreote, A.P.D.; Vaz, M.G.M.V.; Fiore, M.F. Heterocyte-forming cyanobacteria from Brazilian saline-alkaline lakes. *Mol. Phylogenet. Evol.* **2017**, *109*, 105–112. [[CrossRef](#)]
38. Kabirnataj, S.; Nematzadeh, G.A.; Talebi, A.F.; Saraf, A.; Suradkar, A.; Tabatabaei, M.; Singh, P. Description of novel species of *Aliinostoc*, *Desikacharya* and *Desmonostoc* using a polyphasic approach. *Int. J. Syst. Evol. Microbiol.* **2020**, *70*, 3413–3426. [[CrossRef](#)]
39. Kotai, J. Instructions for preparation of modified nutrient solution Z8 for algae. *Nor. Inst. Water Res.* **1972**, *11*, 1–5.
40. Rippka, R. Isolation and purification of cyanobacteria. In *Methods in Enzymology 167*; Academic Press: San Diego, CA, USA, 1988; pp. 3–27.
41. Leber, A.L. Antifungal disk diffusion susceptibility testing. In *Clinical Microbiology Procedures Handbook*; Leber, A.L., Ed.; ASM Press: Washington, DC, USA, 2016; Volume 2.
42. Romo, S.; Perez-Martinez, C. The use of immobilization in alginate beads for long-term storage of *Pseudanabaena galeata* (Cyanobacteria) in the Laboratory. *J. Phycol.* **1997**, *33*, 1073–1076. [[CrossRef](#)]
43. Reynolds, E.S. The use of lead citrate at high pH as an electron-opaque stain in electron microscopy. *J. Cell Biol.* **1963**, *17*, 208–212. [[CrossRef](#)]
44. Boyer, S.L.; Johansen, J.R.; Flechtner, V.R.; Howard, G.L.; Bliss, F. Phylogeny and genetic variance in terrestrial *Microcoleus* (Cyanophyceae) species based on sequence analysis of the 16S rRNA gene and associated 16S–23S ITS region. *J. Phycol.* **2002**, *38*, 1222–1235. [[CrossRef](#)]
45. Taton, A.; Grubisic, S.; Brambilla, E.; De Wit, R.; Willemotte, A. Cyanobacterial diversity in natural and artificial microbial mats of lake Fryxell (McMurdo Dry Valleys, Antarctica): A morphological and molecular approach. *Appl. Environ. Microbiol.* **2003**, *69*, 5157–5169. [[CrossRef](#)]
46. Larkin, M.A.; Blackshields, G.; Brown, N.P.; Chenna, R.; Mcgettigan, P.A.; McWilliam, H.; Valentin, F.; Wallace, I.M.; Wilm, A.; Lopez, R.; et al. Clustal W and Clustal X version 2.0. *Bioinformatics* **2007**, *23*, 2947–2948. [[CrossRef](#)]
47. Akaike, H. A new look at the statistical model identification. *IEEE Trans. Automat. Contr.* **1974**, *19*, 716–723. [[CrossRef](#)]
48. Darriba, D.; Taboada, G.L.; Doallo, R.; Posada, D. JModelTest 2: More models, new heuristics and parallel computing. *Nat. Methods* **2012**, *9*, 772. [[CrossRef](#)] [[PubMed](#)]
49. Ronquist, F.; Teslenko, M.; van der Mark, P.; Ayres, D.L.; Darling, A.; Höhna, S.; Larget, B.; Liu, L.; Suchard, M.A.; Huelsenbeck, J.P. MrBayes 3.2: Efficient bayesian phylogenetic inference and model choice across a large model space. *Syst. Biol.* **2012**, *61*, 539–542. [[CrossRef](#)] [[PubMed](#)]
50. Trifinopoulos, J.; Nguyen, L.-T.; von Haeseler, A.; Minh, B.Q. W-IQ-TREE: A fast online phylogenetic tool for maximum likelihood analysis. *Nucleic Acids Res.* **2016**, *44*, 232–235. [[CrossRef](#)] [[PubMed](#)]
51. Tamura, K.; Stecher, G.; Kumar, S. MEGA11: Molecular Evolutionary Genetics Analysis Version 11. *Mol. Biol. Evol.* **2021**, *38*, 3022–3027. [[CrossRef](#)]
52. Kimura, M. A Simple method for estimating evolutionary rates of base substitutions through comparative studies of nucleotide sequences. *J. Mol. Evol.* **1980**, *16*, 111–120. [[CrossRef](#)]

53. Iteman, I.; Rippka, R.; De Marsac, N.T.; Herdman, M. Comparison of Conserved structural and regulatory domains within divergent 16S rRNA-23S rRNA spacer sequences of cyanobacteria. *Microbiology* **2000**, *146*, 1275–1286. [[CrossRef](#)]
54. Zuker, M. Mfold web server for nucleic acid folding and hybridization prediction. *Nucleic Acids Res.* **2003**, *31*, 3406–3415. [[CrossRef](#)]
55. CLSI. *Performance Standards for Antimicrobial Disk Susceptibility Tests; Approved Standard—Eleventh Edition*. CLSI Document M02-A11, 11th ed.; Clinical and Laboratory Standards Institute: Wayne, PA, USA, 2012.
56. Voráčová, K.; Hájek, J.; Mareš, J.; Urajová, P.; Kuzma, M.; Cheel, J.; Villunger, A.; Kapuscik, A.; Bally, M.; Novák, P.; et al. The cyanobacterial metabolite nocuolin A is a natural oxadiazine that triggers apoptosis in human cancer cells. *PLoS ONE* **2017**, *12*, 1–20. [[CrossRef](#)]
57. Saraf, A.; Dawda, H.G.; Suradkar, A.; Behere, I.; Kotulkar, M.; Shaikh, Z.M.; Kumat, A.; Batule, P.; Mishra, D.; Singh, P. Description of two new species of *Aliinostoc* and one new species of *Desmonostoc* from India based on the polyphasic approach and reclassification of *Nostoc punensis* to *Desmonostoc punense* comb. nov. *FEMS Microbiol. Lett.* **2018**, *365*, 1–10. [[CrossRef](#)]
58. Stackebrandt, E.; Goebel, B.M. Taxonomic Note: A place for DNA-DNA reassociation and 16S rRNA sequence analysis in the present species definition in bacteriology. *Int. J. Syst. Bacteriol.* **1994**, *44*, 846–849. [[CrossRef](#)]
59. Kim, M.; Oh, H.S.; Park, S.C.; Chun, J. Towards a taxonomic coherence between average nucleotide identity and 16S rRNA gene sequence similarity for species demarcation of prokaryotes. *Int. J. Syst. Evol. Microbiol.* **2014**, *64*, 346–351. [[CrossRef](#)]
60. Wilmotte, A.; Neefs, J.M.; De Wachter, R. Evolutionary affiliation of the marine nitrogen-fixing cyanobacterium *Trichodesmium* sp. strain NIBB 1067, derived by 16S ribosomal RNA sequence analysis. *Microbiology* **1994**, *140*, 2159–2164. [[CrossRef](#)]
61. Boyer, S.L.; Flechtner, V.R.; Johansen, J.R. Is the 16S-23S rRNA internal transcribed spacer region a good tool for use in molecular systematics and population genetics? A case study in cyanobacteria. *Mol. Biol. Evol.* **2001**, *18*, 1057–1069. [[CrossRef](#)]
62. Johansen, J.R.; Kovacic, L.; Casamatta, D.A.; Fučíková, K.; Kaštovský, J. Utility of 16S-23S ITS sequence and secondary structure for recognition of intrageneric and intergeneric limits within cyanobacterial taxa: *Leptolyngbya corticola* sp. nov. (Pseudanabaenaceae, Cyanobacteria). *Nov. Hedwigia* **2011**, *92*, 283–302. [[CrossRef](#)]
63. Berrendero Gómez, E.; Johansen, J.R.; Kaštovský, J.; Bohunická, M.; Čapková, K. *Macrochaete* gen. nov. (Nostocales, Cyanobacteria), a taxon morphologically and molecularly distinct from *Calothrix*. *J. Phycol.* **2016**, *52*, 638–655. [[CrossRef](#)]
64. Alvarenga, D.O.; Andreote, A.P.D.; Branco, L.H.Z.; Fiore, M.F. *Kryptousia macronema* gen. nov., sp. nov. and *Kryptousia microlepis* sp. nov., nostoclean cyanobacteria isolated from phyllospheres. *Int. J. Syst. Evol. Microbiol.* **2017**, *67*, 3301–3309. [[CrossRef](#)]
65. Martins, M.D.; Rigonato, J.; Taboga, S.R.; Branco, L.H.Z. Proposal of *Ancylothrix* gen. nov., a new genus of Phormidiaceae (Cyanobacteria, Oscillatoriales) based on a polyphasic approach. *Int. J. Syst. Evol. Microbiol.* **2016**, *66*, 2396–2405. [[CrossRef](#)]
66. Martins, M.D.; Branco, L.H.Z. *Potamolinea* gen. nov. (Oscillatoriales, Cyanobacteria): A phylogenetically and ecologically coherent cyanobacterial genus. *Int. J. Syst. Evol. Microbiol.* **2016**, *66*, 3632–3641. [[CrossRef](#)]
67. Pietrasiak, N.; Reeve, S.; Osorio-Santos, K.; Lipson, D.A.; Johansen, J.R. *Trichotorquatus* gen. nov.—A new genus of soil cyanobacteria discovered from American drylands 1. *J. Phycol.* **2021**, *57*, 886–902. [[CrossRef](#)]
68. Machado-de-Lima, N.M.; Dornelles Martins, M.; Branco, L.H. Description of a tropical new species of *Wilmottia* (Oscillatoriales, Cyanobacteria) and considerations about the monophyly of *W. Murrayi*. *Phytotaxa* **2017**, *307*, 43–54. [[CrossRef](#)]
69. Johansen, J.R.; Mareš, J.; Pietrasiak, N.; Bohunická, M.; Zima, J.; Štenclová, L.; Hauer, T. Highly divergent 16S rRNA sequences in ribosomal operons of *Scytonema hyalinum* (Cyanobacteria). *PLoS ONE* **2017**, *12*, e0186393. [[CrossRef](#)] [[PubMed](#)]
70. Buch, B.; Martins, M.D.; Branco, L.H.Z. A widespread cyanobacterium supported by polyphasic approach: Proposition of *Koimonema perovagatum* gen. & sp. nov. (Oscillatoriales). *J. Phycol.* **2017**, *53*, 1097–1105. [[PubMed](#)]
71. González-Fuente, A.M.; Hernández-Cabanillas, A.; Maderuelo-Corral, S.; Ortega-Doménech, M.; Rosero-Valencia, D.F.; Rumbero-Sánchez, Á.; Tena-Pérez, V. Dihydrooxadiazine Compounds for Treating Infections and Cancer. European Patent EP3156400B1, 15 May 2019.
72. Arunkumar, K.; Selvapalam, N.; Rengasamy, R. The antibacterial compound sulphoglycerolipid 1-0 palmitoyl-3-0(6'-sulpho- $\alpha$ -quinovopyranosyl)-glycerol from *Sargassum wightii* Greville (Phaeophyceae). *Bot. Mar.* **2005**, *48*, 441–445. [[CrossRef](#)]
73. El Baz, F.K.; El Baroty, G.S.; Abd El Baky, H.H.; Abd El-Salam, O.I.; Ibrahim, E.A. Structural characterization and biological activity of sulfolipids from selected marine algae. *Grasas Y Aceites* **2013**, *64*, 561–571.
74. Logan, N.A.; De Vos, P. Bacillus. In *Bergey's Manual of Systematics of Archaea and Bacteria*; Whitman, W.B., Rainey, F., Kämpfer, P., Trujillo, M., Chun, J., DeVos, P., Hedlund, B., Dedysh, S., Eds.; John Wiley & Sons, Ltd.: Chichester, UK, 2015; pp. 1–163.
75. Tidgewell, K.; Clark, B.R.; Gerwick, W.H. The natural products chemistry of cyanobacteria. In *Comprehensive Natural Products II: Chemistry and Biology—Volume 2*; Mander, L., Liu, H.-W., Eds.; Elsevier: Oxford, UK, 2010; pp. 141–188.
76. Tronholm, A.; Engene, N. *Moorena* gen. nov., a valid name for “*Moorea* Engene et al” nom. inval. (Oscillatoriales, Cyanobacteria). *Not. Algarum* **2019**, *122*, 1–2.
77. Trimurtulu, G.; Ohtani, I.; Patterson, G.M.L.; Moore, R.E.; Corbett, T.H.; Valeriote, F.A.; Demchik, L. Total Structures of cryptophycins, potent antitumor depsipeptides from the blue-green alga *Nostoc* sp. strain GSV 224. *J. Am. Chem. Soc.* **1994**, *116*, 4729–4737. [[CrossRef](#)]
78. Magarvey, N.A.; Beck, Z.Q.; Golakoti, T.; Ding, Y.; Huber, U.; Hemscheidt, T.K.; Abelson, D.; Moore, R.E.; Sherman, D.H. Biosynthetic characterization and chemoenzymatic assembly of the cryptophycins. potent anticancer agents from cyanobionts. *ACS Chem. Biol.* **2006**, *1*, 766–779. [[CrossRef](#)]

79. Kang, H.S.; Santarsiero, B.D.; Kim, H.; Krunic, A.; Shen, Q.; Swanson, S.M.; Chai, H.; Kinghorn, A.D.; Orjala, J. Merocyclophanes A and B, antiproliferative cyclophanes from the cultured terrestrial cyanobacterium *Nostoc* sp. *Phytochemistry* **2012**, *79*, 109–115. [[CrossRef](#)]
80. May, D.S.; Chen, W.L.; Lantvit, D.D.; Zhang, X.; Krunic, A.; Burdette, J.E.; Eustaquio, A.; Orjala, J. Merocyclophanes C and D from the cultured freshwater cyanobacterium *Nostoc* sp. (UIC 10110). *J. Nat. Prod.* **2017**, *80*, 1073–1080. [[CrossRef](#)]
81. Kampa, A.; Gagunashvili, A.N.; Gulder, T.A.M.; Morinaka, B.L.; Daolio, C.; Godejohann, M.; Miao, V.P.W.; Piel, J.; Andr sson,  .S. Metagenomic natural product discovery in lichen provides evidence for a family of biosynthetic pathways in diverse symbioses. *Proc. Natl. Acad. Sci. USA* **2013**, *110*, 3129–3137. [[CrossRef](#)]
82. Shishido, T.K.; Popin, R.V.; Jokela, J.; Wahlsten, M.; Fiore, M.F.; Fewer, D.P.; Herfindal, L.; Sivonen, K. Dereplication of natural products with antimicrobial and anticancer activity from Brazilian cyanobacteria. *Toxins* **2019**, *12*, 12. [[CrossRef](#)]
83. Genu rio, D.B.; Silva-Stenico, M.E.; Welker, M.; Beraldo Moraes, L.A.; Fiore, M.F. Characterization of a microcystin and detection of microcystin synthetase genes from a Brazilian isolate of *Nostoc*. *Toxicon* **2010**, *55*, 846–854. [[CrossRef](#)]
84. Armstrong, L.; Vaz, M.G.M.V.; Genu rio, D.B.; Fiore, M.F.; Debonsi, H.M. Volatile compounds produced by cyanobacteria isolated from mangrove environment. *Curr. Microbiol.* **2019**, *76*, 575–582. [[CrossRef](#)]
85. Jokela, J.; Heinil , L.M.P.; Shishido, T.K.; Wahlsten, M.; Fewer, D.P.; Fiore, M.F.; Wang, H.; Haapaniemi, E.; Permi, P.; Sivonen, K. Production of high amounts of hepatotoxin nodularin and new protease inhibitors pseudospumigins by the Brazilian benthic *Nostoc* sp. CENA543. *Front. Microbiol.* **2017**, *8*, 1963. [[CrossRef](#)]
86. Shishido, T.K.; Jokela, J.; Fewer, D.P.; Wahlsten, M.; Fiore, M.F.; Sivonen, K. Simultaneous production of anabaenopeptins and namalides by the cyanobacterium *Nostoc* sp. CENA543. *ACS Chem. Biol.* **2017**, *12*, 2746–2755. [[CrossRef](#)]
87. Bui, H.T.N.; Jansen, R.; Pham, H.T.L.; Mundt, S. Carbamidocyclophanes A-E, chlorinated paracyclophanes with cytotoxic and antibiotic activity from the vietnamese cyanobacterium *Nostoc* sp. *J. Nat. Prod.* **2007**, *70*, 499–503. [[CrossRef](#)]
88. Chlipala, G.E.; Sturdy, M.; Krunic, A.; Lantvit, D.D.; Shen, Q.; Porter, K.; Swanson, S.M.; Orjala, J. Cyliindrocyclophanes with proteasome inhibitory activity from the cyanobacterium *Nostoc* sp. *J. Nat. Prod.* **2010**, *73*, 1529–1537. [[CrossRef](#)]
89. Preisitsch, M.; Harmrolfs, K.; Pham, H.T.; Heiden, S.E.; F ssel, A.; Wiesner, C.; Pretsch, A.; Swiatecka-Hagenbruch, M.; Niedermeyer, T.H.; M ller, R.; et al. Anti-MRSA-acting carbamidocyclophanes H–L from the vietnamese cyanobacterium *Nostoc* sp. CAVN2. *J. Antibiot.* **2015**, *68*, 165–177. [[CrossRef](#)]
90. May, D.S.; Kang, H.-S.; Santarsiero, B.D.; Krunic, A.; Shen, Q.; Burdette, J.E.; Swanson, S.M.; Orjala, J. Ribocyclophanes A–E, glycosylated cyclophanes with antiproliferative activity from two cultured terrestrial cyanobacteria. *J. Nat. Prod.* **2018**, *81*, 572–578. [[CrossRef](#)]
91. Preisitsch, M.; Niedermeyer, T.H.J.; Heiden, S.E.; Neidhardt, I.; Kumpfm ller, J.; Wurster, M.; Harmrolfs, K.; Wiesner, C.; Enke, H.; M ller, R.; et al. Cyliindrofridins A–C, linear cyliindrocyclophane-related alkylresorcinols from the cyanobacterium *Cylindrospermum stagnale*. *J. Nat. Prod.* **2016**, *79*, 106–115. [[CrossRef](#)]
92. Preisitsch, M.; Heiden, S.E.; Beerbaum, M.; Niedermeyer, T.H.J.; Schneefeld, M.; Herrmann, J.; Kumpfm ller, J.; Th rmer, A.; Neidhardt, I.; Wiesner, C.; et al. Effects of halide ions on the carbamidocyclophane biosynthesis in *Nostoc* sp. CAVN2. *Mar. Drugs* **2016**, *14*, 21. [[CrossRef](#)] [[PubMed](#)]
93. Luo, S.; Kang, H.-S.; Krunic, A.; Chlipala, G.E.; Cai, G.; Chen, W.-L.; Franzblau, S.G.; Swanson, S.M.; Orjala, J. Carbamidocyclophanes F and G with anti-*Mycobacterium tuberculosis* activity from the cultured freshwater cyanobacterium *Nostoc* sp. *Tetrahedron Lett.* **2014**, *55*, 686–689. [[CrossRef](#)] [[PubMed](#)]
94. Moore, B.S.; Chen, J.L.; Patterson, G.M.L.; Moore, R.E.; Brinen, L.S.; Kato, Y.; Clardy, J. [7.7]Paracyclophanes from blue-green algae. *J. Am. Chem. Soc.* **1990**, *112*, 4061–4063. [[CrossRef](#)]
95. Moore, B.S.; Chen, J.-L.; Patterson, G.M.L.; Moore, R.E. Structures of cyliindrocyclophanes A-F. *Tetrahedron* **1992**, *48*, 3001–3006. [[CrossRef](#)]
96. Chen, J.L.; Moore, R.E.; Patterson, G.M.L. Structures of nostocyclophanes A-D. *J. Org. Chem.* **1991**, *56*, 4360–4364. [[CrossRef](#)]
97. Bobzin, S.C.; Moore, R.E. Biosynthetic origin of [7.7]Paracyclophanes from Cyanobacteria. *Tetrahedron* **1993**, *49*, 7615–7626. [[CrossRef](#)]
98. Mattila, A.; Andsten, R.-M.; Jumppanen, M.; Assante, M.; Jokela, J.; Wahlsten, M.; Mikula, K.M.; Sigindere, C.; Kwak, D.H.; Gugger, M.; et al. Biosynthesis of the bis-prenylated alkaloids muscoride A and B. *ACS Chem. Biol.* **2019**, *14*, 2683–2690. [[CrossRef](#)]
99. Nagatsu, A.; Kajitani, H.; Sakakibara, J. Muscoride A: A new oxazole peptide alkaloid from freshwater cyanobacterium *Nostoc muscorum*. *Tetrahedron Lett.* **1995**, *36*, 4097–4100. [[CrossRef](#)]
100. Cheel, J.; H jek, J.; Kuzma, M.; Saurav, K.; Sm ykalov , I.; Ondr ckov , E.; Urajov , P.; Vu, D.L.; Faure, K.; Kopeck , J.; et al. Application of HPLC combined with polymeric resins and HPLC for the separation of cyclic lipopeptides muscotoxins A-C and their antimicrobial activity. *Molecules* **2018**, *23*, 2653. [[CrossRef](#)]